Preprint (2025) 1–20

Two-derivative schemes for low-Mach flows

Arjun Thenery Manikantan[a], Jochen Schütz[a]

[a]*Faculty of Sciences & Data Science Institute, Hasselt University, Agoralaan Gebouw D, BE-3590 Diepenbeek, Belgium*

Abstract

In this paper, we analyze two-derivative IMEX (implicit/explicit) schemes applied to the isentropic Euler equations. In particular, we investigate a broad range of stiffness, varying from a weakly compressible regime ($\varepsilon \ll 1$) to a fully compressible regime ($\varepsilon \approx 1$). The high-order discontinuous Galerkin spectral element method is used as spatial discretization. We prove that the considered two-derivative IMEX schemes for the splitting described in [Degond, Tang, 2011] are asymptotically preserving. We show experimentally that the schemes are stable and convergent under a convective CFL condition independent of the stiffness parameter ε.

Keywords: Asymptotic preserving, isentropic Euler, IMEX schemes, discontinuous Galerkin, predictor-corrector schemes

1. Introduction

Solving partial differential equations (PDE) is an ubiquitous task in computational modelling of all sorts of physical phenomena. In particular, it is of greatest importance in fluid dynamics. Approximating PDEs is a widely studied field, yet there are still open issues and challenges. Solving time-dependent conservation equations in fluid dynamics is highly demanding and, at the same time, computationally expensive. Therefore, new strategies that utilize the most modern computational architecture are constantly being developed. Generally, the procedure of finding a numerical solution to these equations starts with discretizing the spatial derivatives in the PDE, resulting in a time-dependent system of ordinary differential equations (ODE). Then, well-suited timestepping procedures are employed to solve this system of ODEs numerically.

In many cases, this ODE is stiff, with stiffness arising from, e.g., the equations themselves or the spatial discretization. Typically, stiffness manifests itself through vast differences in orders of magnitude of the eigenvalues of the underlying system. In this work, we consider a model for compressible flow of form

$$\mathbf{w}_t + \nabla \cdot \mathbf{F}(\mathbf{w}) = 0, \tag{1}$$

with a flux term $\mathbf{F}(\mathbf{w})$ that depends on a parameter ε, see Eq. (3). In this prototypical equation, the stiffness is characterized by this parameter ε. In particular, for $\varepsilon \to 0$, the eigenvalues are of vastly different size, see Eq. (4).

Widely used timestepping schemes for compressible fluid equations are explicit schemes due to their easy implementation and their high efficiency for non-stiff equations. However, the stability restriction that arises from the CFL conditions [1] can often force unfeasible bounds on the timestep size. In the case of equation (3), it mandates choosing the timestep size Δt to be $O(\varepsilon \Delta x)$, where Δx is the spatial mesh size. Hence, it is impractical to use a timestep

$$\Delta t = O(\varepsilon \Delta x), \quad \text{as} \quad \varepsilon \to 0.$$

Email addresses: arjun.thenerymanikantan@uhasselt.be (Arjun Thenery Manikantan), jochen.schuetz@uhasselt.be (Jochen Schütz)

In this situation, using implicit timestepping schemes [2] helps to overcome timestep restrictions. However, it brings on the cumbersome task of solving large non-linear algebraic systems of equations. Additionally, if the fluxes are highly non-linear and/or very stiff, the implicit solver may require many iterations to converge (or not converge at all), resulting in a longer execution time for the timestepping scheme.

Considering the challenges of timestepping schemes mentioned above, methods that simultaneously leverage the computational efficiency of an explicit scheme and the unconstrained timestep size requirement from implicit schemes are highly demanding. The aforementioned methods that use a split flux evaluation are the implicit-explicit (IMEX) time-stepping schemes, see, e.g., [3, 4, 5, 6, 7, 8]. The flux function is generally split into stiff and non-stiff parts, i.e.,

$$\mathbf{w}_t + \nabla \cdot \Big(\underbrace{\mathbf{F}_{\mathrm{I}}(\mathbf{w})}_{\text{stiff}} + \underbrace{\mathbf{F}_{\mathrm{E}}(\mathbf{w})}_{\text{non-stiff}} \Big) = 0. \tag{2}$$

Then, the stiff and non-stiff parts are evaluated implicitly and explicitly, respectively. The effective way would be to choose a (nearly) linear stiff part, making the implicit solver work faster, and a non-stiff part, which can give a more reasonable timestep restriction that is independent of ε, i.e.,

$$\Delta t = O(\Delta x).$$

Classical time integration schemes are of the one-derivative type, i.e., they rely on the first temporal derivative ($\mathbf{w}_t$) of the problem only. Adding intermediate stages or utilizing solutions from the previous timesteps is the only way to increase their order of convergence. Devising higher-order schemes using these often come with the strenuous chore of solving many order conditions. Also, utilizing solutions from previous timesteps beyond a threshold can severely affect stability properties. Considering multi-derivative schemes results in fewer order conditions and more flexibility over coefficients that are to be found. This class of schemes utilizes higher-order derivatives of the problem ($\mathbf{w}_{tt}$ and more), see Eq. (8). For some schemes, we refer to [9, 10, 11, 12, 13, 14] and [15, 16, 17] for some IMEX multi-derivative schemes.

In [15], a two-derivative asymptotic preserving (AP) IMEX scheme for ordinary differential equations that works in a predictor-corrector fashion has been developed. The scheme has been extended later, see [18, 19, 20], and termed Hermite-Birkhoff Predictor-Corrector (HBPC) scheme. Generally, higher-order methods are designed to give highly accurate numerical solutions even with relatively large timestep sizes, provided the scheme remains stable. When solving PDEs, the higher-order time stepping schemes are to be combined with higher-order spatial discretizations for highly accurate numerical solutions. In [18, 21], the authors have combined HBPC scheme with the higher-order Discontinuous Galerkin Spectral Element Methods (DGSEM) [22] for viscous compressible flow equations

When numerically solving the singularly perturbed problem (3) for $\varepsilon \ll 1$, there is the additional difficulty that for $\varepsilon \to 0$, the equations change type (hence singularly perturbed). To be efficient and stable, both temporal and spatial discretization must take this behavior into account, a property that is called 'asymptotic preservation' (AP) [23, 24, 25, 26, 15]. An asymptotically preserving scheme means that the limit of the numerical solution of the singularly perturbed problem as $\varepsilon \to 0$ is consistent with the solution in the singular limit of the problem (6) for finite values of Δt and Δx.

In this paper, we analyze and showcase the effect of IMEX-HBPC schemes [15, 18, 27] combined with DGSEM [22] spatial discretization on the low-Mach isentropic Euler equations. Considering the reference Mach number ε, the latter are given by

$$\mathbf{w}_t + \nabla \cdot \mathbf{F}(\mathbf{w}) = 0, \quad \text{where} \quad \mathbf{w} = \begin{pmatrix} \rho \\ \rho \mathbf{v} \end{pmatrix} \quad \text{and} \quad \mathbf{F}(\mathbf{w}) = \begin{pmatrix} \rho \mathbf{v} \\ \rho \mathbf{v} \otimes \mathbf{v} + \frac{p}{\varepsilon^2} \mathbf{Id} \end{pmatrix}. \tag{3}$$

The system is closed with the equation of state $p(\rho) := \kappa \rho^\gamma$, where $\kappa > 0$ and $\gamma > 1$. The eigenvalues of the Jacobian in the direction of some vector $\mathbf{n}$, i.e., $\left(\frac{\partial F}{\partial \mathbf{w}} \cdot \mathbf{n}\right)$ are in two dimensions given by

$$\lambda_1 = \mathbf{v} \cdot \mathbf{n} \quad \text{and} \quad \lambda_{2,3} = \mathbf{v} \cdot \mathbf{n} \pm \frac{1}{\varepsilon} \sqrt{\kappa \gamma \rho^{\gamma - 1}}. \tag{4}$$

To achieve a well-behaved limit of Eq. (3) as $\varepsilon \to 0$ [28], we consider well-prepared initial data

$$\rho \,\big|_{t=0} = \text{const} + O(\varepsilon^2) \quad \text{and} \quad \nabla \cdot (\rho \mathbf{v}) \,\big|_{t=0} = O(\varepsilon), \tag{5}$$

and we assume that the solution $\mathbf{w}$ of (3) has a Hilbert expansion, given by

$$\mathbf{w} = \mathbf{w}_{(0)} + \varepsilon \mathbf{w}_{(1)} + \varepsilon^2 \mathbf{w}_{(2)} + O(\varepsilon^3).$$

Formally, for $\varepsilon \to 0$, (3) yields the incompressible Euler equations given by

$$\begin{aligned} \rho_{(0)} \equiv \text{const} > 0, \quad \nabla \cdot \mathbf{v}_{(0)} = 0, \\ (\mathbf{v}_{(0)})_t + \nabla \cdot (\mathbf{v}_{(0)} \otimes \mathbf{v}_{(0)}) + \frac{\nabla p_{(2)}}{\rho_{(0)}} = 0. \end{aligned} \tag{6}$$

There exist several well-studied splittings $\mathbf{F}_\mathrm{I}$ and $\mathbf{F}_\mathrm{E}$ in literature [29, 30, 31]. In particular, we use the splitting of [29] in this work, given by

$$\mathbf{F}_\mathrm{I}(\mathbf{w}) = \begin{pmatrix} \rho \mathbf{v} \\ \frac{1-\varepsilon^2}{\varepsilon^2} p \mathbf{Id} \end{pmatrix} \quad \text{and} \quad \mathbf{F}_\mathrm{E}(\mathbf{w}) = \begin{pmatrix} \rho \mathbf{v} \\ \rho \mathbf{v} \otimes \mathbf{v} + p \mathbf{Id} \end{pmatrix}.$$

We show that the combination of HBPC with DGSEM, applied to this splitting, results in an asymptotically preserving algorithm. To our knowledge, this is the first result in this direction for a two-derivative scheme. The result can be extended to more elaborate equations representing compressible flow.

The sections of this paper are structured as follows: In Sec. 2, we introduce the two-derivative IMEX-Taylor method followed by the semi-discrete and fully-discrete analysis of the method in Sec. 2.1 and Sec. 2.2 to show the asymptotic preservation. Then, the AP analysis of the IMEX-HBPC schemes is given in Sec. 3. Numerical results are shown in Sec. 5. The paper concludes in Sec. 6 with an outlook.

2. Two-derivative IMEX-Taylor method

The PDE (1) can be formally cast into an ODE of form

$$\mathbf{w}_t = -\nabla \cdot \mathbf{F}(\mathbf{w}) =: \mathbf{R}^{(1)}(\mathbf{w}), \tag{7}$$

in some infinite dimensional space. The timestepping schemes considered in this work require the second time derivative of the equation. Hence, we have

$$\mathbf{w}_{tt} = \Big(-\nabla \cdot \mathbf{F}(\mathbf{w}) \Big)_t = -\nabla \cdot \left(\frac{\partial \mathbf{F}(\mathbf{w})}{\partial \mathbf{w}} \mathbf{w}_t \right) = -\nabla \cdot \left(\frac{\partial \mathbf{F}(\mathbf{w})}{\partial \mathbf{w}} \mathbf{R}^{(1)}(\mathbf{w}) \right) =: \mathbf{R}^{(2)}(\mathbf{w}). \tag{8}$$

Consider a general splitting of the flux term in (3) into implicit (**I**) and explicit (**E**) parts, given by

$$\mathbf{F}(\mathbf{w}) = \mathbf{F}_\mathrm{I}(\mathbf{w}) + \mathbf{F}_\mathrm{E}(\mathbf{w}). \tag{9}$$

Then, in Tab. 1, we define similar notations as in Eqs. (7) and (8) for the split flux (9). Using the definitions from Tab. 1, we have the split flux PDE cast into the ODE

$$\mathbf{w}_t = \mathbf{R}_\mathrm{I}^{(1)}(\mathbf{w}) + \mathbf{R}_\mathrm{E}^{(1)}(\mathbf{w}), \tag{10}$$

for the first derivative and

$$\mathbf{w}_{tt} = \mathbf{R}_\mathrm{I}^{(2)}(\mathbf{w}, \mathbf{w}) + \mathbf{R}_\mathrm{E}^{(2)}(\mathbf{w}), \tag{11}$$

for the second derivative.

Remark 1. *The idea of an IMEX time-stepping schemes is that the explicit flux terms are never inverted. However, when it comes to multi-derivative schemes, the derivatives of the implicit flux term are forced to carry contributions from the explicit flux due to their definition, as in the implicit part of* $\mathbf{w}_{tt}$ *given by*

$$-\nabla \cdot \left(\frac{\partial \mathbf{F}_I(\mathbf{w})}{\partial \mathbf{w}} \Big(\mathbf{R}_I^{(1)}(\mathbf{w}) + \mathbf{R}_E^{(1)}(\mathbf{w}) \Big) \right). \tag{12}$$

Notation	Definition w.r.t a general splitting
$\mathbf{R}^{(1)}(\mathbf{w})$	$-\nabla \cdot \mathbf{F}(\mathbf{w})$
$\mathbf{R}_{\mathrm{E}}^{(1)}(\mathbf{w})$	$-\nabla \cdot \mathbf{F}_{\mathrm{E}}(\mathbf{w})$
$\mathbf{R}_{\mathrm{I}}^{(1)}(\mathbf{w})$	$-\nabla \cdot \mathbf{F}_{\mathrm{I}}(\mathbf{w})$
$\mathbf{R}^{(2)}(\mathbf{w})$	$-\nabla \cdot \left(\frac{\partial \mathbf{F}(\mathbf{w})}{\partial \mathbf{w}} \mathbf{R}^{(1)}(\mathbf{w})\right)$
$\mathbf{R}_{\mathrm{E}}^{(2)}(\mathbf{w})$	$-\nabla \cdot \left(\frac{\partial \mathbf{F}_{\mathrm{E}}(\mathbf{w})}{\partial \mathbf{w}} \mathbf{R}^{(1)}(\mathbf{w})\right) = -\nabla \cdot \left(\frac{\partial \mathbf{F}_{\mathrm{E}}(\mathbf{w})}{\partial \mathbf{w}} \left(\mathbf{R}_{\mathrm{I}}^{(1)}(\mathbf{w}) + \mathbf{R}_{\mathrm{E}}^{(1)}(\mathbf{w})\right)\right)$
$\mathbf{R}_{\mathrm{I}}^{(2)}(\bar{\mathbf{w}}, \mathbf{w})$	$-\nabla \cdot \left(\frac{\partial \mathbf{F}_{\mathrm{I}}(\mathbf{w})}{\partial \mathbf{w}} \left(\mathbf{R}_{\mathrm{I}}^{(1)}(\mathbf{w}) + \mathbf{R}_{\mathrm{E}}^{(1)}(\bar{\mathbf{w}})\right)\right)$, (Refer to Rem. 1)

Table 1. Definitions of notations used in paper.

Hence, the term (12) *indirectly inverts the explicit flux contributions, adversely affecting the schemes. To tackle this condition of the explicit flux contribution on the higher derivatives of the implicit flux terms, the authors in [27] have introduced a slightly modified definition of the implicit part of* $\mathbf{w}_{tt}$ *for the use in IMEX schemes. It is given by*

$$-\nabla \cdot \left(\frac{\partial \mathbf{F}_I(\mathbf{w})}{\partial \mathbf{w}} \left(\mathbf{R}_I^{(1)}(\mathbf{w}) + \mathbf{R}_E^{(1)}(\bar{\mathbf{w}})\right)\right) =: \mathbf{R}_I^{(2)}(\bar{\mathbf{w}}, \mathbf{w}), \tag{13}$$

where $\bar{\mathbf{w}}$ *will be an* explicitly known *value in the algorithm, hence preventing explicit contributions from getting inverted, see, e.g., Eq.* (14) *below this remark. We utilize the latter definition* (13) *for the implicit part of* $\mathbf{w}_{tt}$ *in all the schemes and its analysis provided in the paper.*

Algorithm 1 (Two-derivative IMEX-Taylor)**.** *Given the solution* $\mathbf{w}^n$ *at time instance* t^n*, the solution update at* t^{n+1} *by the two-derivative IMEX-Taylor method is given by*

$$\mathbf{w}^{n+1} := \mathbf{w}^n + \Delta t \left[\mathbf{R}_E^{(1)}(\mathbf{w}^n) + \mathbf{R}_I^{(1)}(\mathbf{w}^{n+1})\right] + \frac{\Delta t^2}{2} \left[\mathbf{R}_E^{(2)}(\mathbf{w}^n) - \mathbf{R}_I^{(2)}(\mathbf{w}^n, \mathbf{w}^{n+1})\right]. \tag{14}$$

2.1. Semi-discrete asymptotic analysis

We assume that the differential equations are defined on the domain $\Omega \times [0, T_{end}]$ with $\Omega \subset \mathbb{R}^2$ and periodic boundary conditions. As already mentioned, we consider the splitting from [29] (called DeTa in the sequel),

$$\underbrace{\begin{pmatrix} \rho \\ \rho \mathbf{v} \end{pmatrix}_t}_{\mathbf{w}_t} + \nabla \cdot \underbrace{\begin{pmatrix} \rho \mathbf{v} \\ \frac{1-\varepsilon^2}{\varepsilon^2} p \mathbf{Id} \end{pmatrix}}_{\mathbf{F}_{\mathrm{I}}(\mathbf{w})} + \nabla \cdot \underbrace{\begin{pmatrix} 0 \\ \rho \mathbf{v} \otimes \mathbf{v} + p \mathbf{Id} \end{pmatrix}}_{\mathbf{F}_{\mathrm{E}}(\mathbf{w})} = 0. \tag{15}$$

Take $\mathbf{w} = (\rho, u, v)^T$ and $\bar{\mathbf{w}} = (\bar{\rho}, \bar{u}, \bar{v})^T$ with the pressures p and $\bar{p}$ respectively. The derivative of the pressure term is denoted as $p' = \kappa\gamma\rho^{\gamma-1}$. Expanded definitions of the divergence terms mentioned in Tab. 1 for the DeTa splitting (15) are given in Tab. 2.

Consider the asymptotic expansion ($\varepsilon < 1$) of the numerical solution, i.e.,

$$\mathbf{w}^{n+1} = \mathbf{w}_{(0)}^{n+1} + \varepsilon \mathbf{w}_{(1)}^{n+1} + \varepsilon^2 \mathbf{w}_{(2)}^{n+1} + O(\varepsilon^3)$$

assuming a well-prepared solution at t^n, i.e.,

$$\rho^n = \text{const} + O(\varepsilon^2) \quad \text{and} \quad \nabla \cdot (\rho \mathbf{v})^n = O(\varepsilon).$$

Notation	Definition w.r.t DeTa splitting (15)
$\mathbf{R}^{(1)}(\mathbf{w})$	$-\begin{pmatrix} \rho u \\ \rho u^2 + \frac{1}{\varepsilon^2} p \\ \rho uv \end{pmatrix}_x - \begin{pmatrix} \rho v \\ \rho uv \\ \rho v^2 + \frac{1}{\varepsilon^2} p \end{pmatrix}_y$
$\mathbf{R}^{(1)}_{\mathrm{E}}(\mathbf{w})$	$-\begin{pmatrix} 0 \\ \rho u^2 + p \\ \rho uv \end{pmatrix}_x - \begin{pmatrix} 0 \\ \rho uv \\ \rho v^2 + p \end{pmatrix}_y$
$\mathbf{R}^{(1)}_{\mathrm{I}}(\mathbf{w})$	$-\begin{pmatrix} \rho u \\ \frac{1-\varepsilon^2}{\varepsilon^2} p \\ 0 \end{pmatrix}_x - \begin{pmatrix} \rho v \\ 0 \\ \frac{1-\varepsilon^2}{\varepsilon^2} p \end{pmatrix}_y$
$\mathbf{R}^{(2)}(\mathbf{w})$	$\begin{pmatrix} \left(\rho u^2 + \frac{p}{\varepsilon^2}\right)_x + (\rho uv)_y \\ \left(-u^2 + \frac{p'}{\varepsilon^2}\right)\left((\rho u)_x + (\rho v)_y\right) + 2u\left(\left(\rho u^2 + \frac{p}{\varepsilon^2}\right)_x + (\rho uv)_y\right) \\ -uv\left((\rho u)_x + (\rho v)_y\right) + v\left(\left(\rho u^2 + \frac{p}{\varepsilon^2}\right)_x + (\rho uv)_y\right) + u\left((\rho uv)_x + \left(\rho v^2 + \frac{p}{\varepsilon^2}\right)_y\right) \end{pmatrix}_x + \begin{pmatrix} (\rho uv)_x + \left(\rho v^2 + \frac{p}{\varepsilon^2}\right)_y \\ -uv\left((\rho u)_x + (\rho v)_y\right) + v\left(\left(\rho u^2 + \frac{p}{\varepsilon^2}\right)_x + (\rho uv)_y\right) + u\left((\rho uv)_x + \left(\rho v^2 + \frac{p}{\varepsilon^2}\right)_y\right) \\ \left(-v^2 + \frac{p'}{\varepsilon^2}\right)\left((\rho u)_x + (\rho v)_y\right) + 2v\left((\rho uv)_x + \left(\rho v^2 + \frac{p}{\varepsilon^2}\right)_y\right) \end{pmatrix}_y$
$\mathbf{R}^{(2)}_{\mathrm{E}}(\mathbf{w})$	$\begin{pmatrix} 0 \\ \left(-u^2 + p'\right)\left((\rho u)_x + (\rho v)_y\right) + 2u\left(\left(\rho u^2 + \frac{p}{\varepsilon^2}\right)_x + (\rho uv)_y\right) \\ -uv\left((\rho u)_x + (\rho v)_y\right) + v\left(\left(\rho u^2 + \frac{p}{\varepsilon^2}\right)_x + (\rho uv)_y\right) + u\left((\rho uv)_x + \left(\rho v^2 + \frac{p}{\varepsilon^2}\right)_y\right) \end{pmatrix}_x + \begin{pmatrix} 0 \\ -uv\left((\rho u)_x + (\rho v)_y\right) + v\left(\left(\rho u^2 + \frac{p}{\varepsilon^2}\right)_x + (\rho uv)_y\right) + u\left((\rho uv)_x + \left(\rho v^2 + \frac{p}{\varepsilon^2}\right)_y\right) \\ \left(-v^2 + p'\right)\left((\rho u)_x + (\rho v)_y\right) + 2v\left((\rho uv)_x + \left(\rho v^2 + \frac{p}{\varepsilon^2}\right)_y\right) \end{pmatrix}_y$
$\mathbf{R}^{(2)}_{\mathrm{I}}(\bar{\mathbf{w}}, \mathbf{w})$	$\begin{pmatrix} \frac{1-\varepsilon^2}{\varepsilon^2} p_x + \left(\left(\bar{\rho}\bar{u}^2 + \bar{p}\right)_x + (\bar{\rho}\bar{u}\bar{v})_y\right) \\ \frac{1-\varepsilon^2}{\varepsilon^2} p'\left((\rho u)_x + (\rho v)_y\right) \\ 0 \end{pmatrix}_x + \begin{pmatrix} \frac{1-\varepsilon^2}{\varepsilon^2} p_y + \left((\bar{\rho}\bar{u}\bar{v})_x + \left(\bar{\rho}\bar{v}^2 + \bar{p}\right)_y\right) \\ 0 \\ \frac{1-\varepsilon^2}{\varepsilon^2} p'\left((\rho u)_x + (\rho v)_y\right) \end{pmatrix}_y$

Table 2. Expansion of the divergence terms mentioned in Tab. 1 for the DeTa splitting (15). Let $\mathbf{w} = (\rho, u, v)^T$ and $\bar{\mathbf{w}} = (\bar{\rho}, \bar{u}, \bar{v})^T$ with the pressures p and $\bar{p}$ respectively. The derivative of the pressure is denoted as p', where $p' = \kappa\gamma\rho^{\gamma-1}$.

Theorem 1. *The two-derivative IMEX-Taylor method combined with the DeTa splitting (15) is AP in the sense that the formal limit $\varepsilon \to 0$ of the numerical solution using (14), with well-prepared initial data and periodic boundary conditions, is a consistent discretization of the incompressible Euler equations (6).*

Proof. The proof of the theorem is a direct consequence of the following Lemmas 1, 2 and 3. Lemma 1 and Lemma 2 show the well-prepared property of the updated solution at t^{n+1}. Lemma 3 shows that the limiting method is the

consistent semi-discretization of the limiting equation. □

Substituting the corresponding flux terms from Tab. 2 in the time-stepping scheme (14), we get

$$
\begin{aligned}
\begin{pmatrix}\rho\\ \rho u\\ \rho v\end{pmatrix}^{n+1} = \begin{pmatrix}\rho\\ \rho u\\ \rho v\end{pmatrix}^{n} - \Delta t \Bigg(& \underbrace{\begin{pmatrix}(\rho u)_x + (\rho v)_y\\ \frac{1-\varepsilon^2}{\varepsilon^2} p_x\\ \frac{1-\varepsilon^2}{\varepsilon^2} p_y\end{pmatrix}^{n+1}}_{-\mathbf{R}_{\mathrm{I}}^{(1)}(\mathbf{w}^{n+1})} + \underbrace{\begin{pmatrix}0\\ \left(\rho u^2 + p\right)_x + (\rho u v)_y\\ (\rho u v)_x + \left(\rho v^2 + p\right)_y\end{pmatrix}^{n}}_{-\mathbf{R}_{\mathrm{E}}^{(1)}(\mathbf{w}^{n})} \Bigg) \\
& - \frac{\Delta t^2}{2} \Bigg(\underbrace{\begin{pmatrix}\left\{\frac{1-\varepsilon^2}{\varepsilon^2} p_x\right\}^{n+1} + \left\{\left(\rho u^2 + p\right)_x + (\rho u v)_y\right\}^{n}\\ \left\{\frac{1-\varepsilon^2}{\varepsilon^2} p' \left((\rho u)_x + (\rho v)_y\right)\right\}^{n+1}\\ 0\end{pmatrix}_x + \begin{pmatrix}\left\{\frac{1-\varepsilon^2}{\varepsilon^2} p_y\right\}^{n+1} + \left\{(\rho u v)_x + \left(\rho v^2 + p\right)_y\right\}^{n}\\ 0\\ \left\{\frac{1-\varepsilon^2}{\varepsilon^2} p' \left((\rho u)_x + (\rho v)_y\right)\right\}^{n+1}\end{pmatrix}_y}_{\mathbf{R}_{\mathrm{I}}^{(2)}(\mathbf{w}^{n},\mathbf{w}^{n+1})} \Bigg) \\
& + \frac{\Delta t^2}{2} \Bigg(\underbrace{\begin{pmatrix}0\\ \left(-u^2 + p'\right)\left((\rho u)_x + (\rho v)_y\right) + 2u\left(\left(\rho u^2 + \frac{p}{\varepsilon^2}\right)_x + (\rho u v)_y\right)\\ -uv\left((\rho u)_x + (\rho v)_y\right) + v\left(\left(\rho u^2 + \frac{p}{\varepsilon^2}\right)_x + (\rho u v)_y\right) + u\left((\rho u v)_x + \left(\rho v^2 + \frac{p}{\varepsilon^2}\right)_y\right)\end{pmatrix}_x^{n}}_{\mathbf{R}_{\mathrm{E}}^{(2)}(\mathbf{w}^{n})} \\
& \qquad + \underbrace{\begin{pmatrix}0\\ -uv\left((\rho u)_x + (\rho v)_y\right) + v\left(\left(\rho u^2 + \frac{p}{\varepsilon^2}\right)_x + (\rho u v)_y\right) + u\left((\rho u v)_x + \left(\rho v^2 + \frac{p}{\varepsilon^2}\right)_y\right)\\ \left(-v^2 + p'\right)\left((\rho u)_x + (\rho v)_y\right) + 2v\left((\rho u v)_x + \left(\rho v^2 + \frac{p}{\varepsilon^2}\right)_y\right)\end{pmatrix}_y^{n}}_{\mathbf{R}_{\mathrm{E}}^{(2)}(\mathbf{w}^{n})} \Bigg) .
\end{aligned}
\tag{16}
$$

Lemma 1. *The quantities $\rho_{(0)}^{n+1}$ and $\rho_{(1)}^{n+1}$ in the asymptotic expansion of ρ^{n+1} in Eq. (16) are constant in space, with an assumption of well prepared solution at t^n and periodic boundary conditions.*

Proof. Consider the $O(\varepsilon^{-2})$ terms from (16) with well-preparedness assumption on $\mathbf{w}^n$. From the density equation, we have

$$
\partial_{xx} p_{(0)}^{n+1} + \partial_{yy} p_{(0)}^{n+1} = 0 \tag{17}
$$

and from the momentum equations, we have

$$
\begin{aligned}
-\Delta t \partial_x p_{(0)}^{n+1} - \frac{\Delta t^2}{2} \partial_x \left(p'_{(0)} \left((\rho_{(0)} u_{(0)})_x + (\rho_{(0)} v_{(0)})_y \right) \right)^{n+1} = 0 \\
-\Delta t \partial_y p_{(0)}^{n+1} - \frac{\Delta t^2}{2} \partial_y \left(p'_{(0)} \left((\rho_{(0)} u_{(0)})_x + (\rho_{(0)} v_{(0)})_y \right) \right)^{n+1} = 0.
\end{aligned}
\tag{18}
$$

Similarly considering the $O(\varepsilon^{-1})$ terms, we get

$$
\partial_{xx} p_{(1)}^{n+1} + \partial_{yy} p_{(1)}^{n+1} = 0 \tag{19}
$$

from the density equation and,

$$
\begin{aligned}
-\Delta t \partial_x p_{(1)}^{n+1} - \frac{\Delta t^2}{2} \partial_x \left(p'_{(1)} \left((\rho_{(0)} u_{(0)})_x + (\rho_{(0)} v_{(0)})_y \right) + p'_{(0)} \left((\rho_{(0)} u_{(1)} + \rho_{(1)} u_{(0)})_x + (\rho_{(0)} v_{(1)} + \rho_{(1)} v_{(0)})_y \right) \right)^{n+1} = 0 \\
-\Delta t \partial_y p_{(1)}^{n+1} - \frac{\Delta t^2}{2} \partial_y \left(p'_{(1)} \left((\rho_{(0)} u_{(0)})_x + (\rho_{(0)} v_{(0)})_y \right) + p'_{(0)} \left((\rho_{(0)} u_{(1)} + \rho_{(1)} u_{(0)})_x + (\rho_{(0)} v_{(1)} + \rho_{(1)} v_{(0)})_y \right) \right)^{n+1} = 0
\end{aligned}
\tag{20}
$$

from the momentum equations. The $O(1)$ term from the density equation gives

$$
\begin{aligned}
\rho_{(0)}^{n+1} = \rho_{(0)}^{n} - \Delta t \left((\rho_{(0)} u_{(0)})_x + (\rho_{(0)} v_{(0)})_y \right)^{n+1} & - \frac{\Delta t^2}{2} \left(\partial_{xx} p_{(2)}^{n+1} + \partial_x \left(\left(\rho_{(0)} u_{(0)}^2\right)_x + (\rho_{(0)} u_{(0)} v_{(0)})_y \right)^{n} \right) \\
& - \frac{\Delta t^2}{2} \left(\partial_{yy} p_{(2)}^{n+1} + \partial_y \left((\rho_{(0)} u_{(0)} v_{(0)})_x + \left(\rho_{(0)} v_{(0)}^2\right)_y \right)^{n} \right),
\end{aligned}
\tag{21}
$$

considering well-prepared assumptions at t^n. Since the boundary conditions are set to be periodic, it implies the existence of Fourier series expansion for $\rho_{(0)}^{n+1}$ and $\rho_{(1)}^{n+1}$. Substituting the Fourier series solution in (17) and (19) forces zero values to the Fourier coefficients. Hence it can be proved that the solutions to (17) and (19) are independent of space variables. Therefore the equation of state $p(\rho) := \kappa\rho^\gamma$ implies that density terms $\rho_{(0)}^{n+1}$ and $\rho_{(1)}^{n+1}$ are independent of space variables.
Now integrating Eq. (21) over the spatial domain, we obtain

$$\int_\Omega \frac{\rho_{(0)}^{n+1} - \rho_{(0)}^{n}}{\Delta t} = -\int_\Omega \rho_{(0)}^{n+1}\, \nabla\cdot(\mathbf{v}_{(0)})^{n+1} - \frac{\Delta t}{2}\int_\Omega \nabla\cdot(\nabla p_{(2)})^{n+1} - \frac{\Delta t}{2}\int_\Omega \rho_{(0)}^{n}\, \nabla\cdot\left(\left(u_{(0)}^2\right)_x + (u_{(0)}v_{(0)})_y, (u_{(0)}v_{(0)})_x + \left(v_{(0)}^2\right)_y\right)^n$$

$$\left(\rho_{(0)}^{n+1} - \rho_{(0)}^{n}\right)\frac{|\Omega|}{\Delta t} = -\rho_{(0)}^{n+1}\int_{\partial\Omega} \mathbf{n}\cdot\mathbf{v}_{(0)}^{n+1} - \frac{\Delta t}{2}\int_{\partial\Omega}\mathbf{n}\cdot(\nabla p_{(2)})^{n+1} - \frac{\Delta t}{2}\rho_{(0)}^{n}\int_{\partial\Omega}\mathbf{n}\cdot\left(\left(u_{(0)}^2\right)_x + (u_{(0)}v_{(0)})_y, (u_{(0)}v_{(0)})_x + \left(v_{(0)}^2\right)_y\right)^n$$

$$\Rightarrow \quad \rho_{(0)}^{n+1} - \rho_{(0)}^{n} = 0 \quad (\textit{due to periodic boundary conditions}). \tag{22}$$

Similarly using the $O(\varepsilon)$ terms from the density equation we can obtain

$$\rho_{(1)}^{n+1} - \rho_{(1)}^{n} = 0. \tag{23}$$

Hence from Eq. (22) and Eq. (23),we get

$$\rho^{n+1} = \text{const} + O(\varepsilon^2). \tag{24}$$

□

Lemma 2. *The quantity $\mathbf{v}_{(0)}^{n+1}$ is divergence free under the assumptions of Lemma 1.*

Proof. From Eq. (18), we get

$$\left.\begin{aligned}\partial_x\left((u_{(0)})_x + (v_{(0)})_y\right)^{n+1} &= 0\\ \partial_y\left((u_{(0)})_x + (v_{(0)})_y\right)^{n+1} &= 0\end{aligned}\right\} \Rightarrow \nabla\cdot\mathbf{v}_{(0)}^{n+1} = C,$$

where C is a constant. Now substituting $\nabla\cdot\mathbf{v}_{(0)}^{n+1} = C$ in (21) and integrating over the spatial domain gives

$$0 = -\int_\Omega \rho_{(0)}^{n+1}\, C - \frac{\Delta t}{2}\int_\Omega \nabla\cdot(\nabla p_{(2)})^{n+1} - \frac{\Delta t}{2}\int_\Omega \rho_{(0)}^{n}\, \nabla\cdot\left(\left(u_{(0)}^2\right)_x + (u_{(0)}v_{(0)})_y, (u_{(0)}v_{(0)})_x + \left(v_{(0)}^2\right)_y\right)^n$$

$$0 = -\rho_{(0)}^{n+1} C\,|\Omega| - \frac{\Delta t}{2}\int_{\partial\Omega}\mathbf{n}\cdot(\nabla p_{(2)})^{n+1} - \frac{\Delta t}{2}\rho_{(0)}^{n}\int_{\partial\Omega}\mathbf{n}\cdot\left(\left(u_{(0)}^2\right)_x + (u_{(0)}v_{(0)})_y, (u_{(0)}v_{(0)})_x + \left(v_{(0)}^2\right)_y\right)^n$$

$$\Rightarrow \quad 0 = C \quad (\textit{due to periodic boundary conditions}).$$

Hence we get

$$\nabla\cdot\mathbf{v}^{n+1} = O(\varepsilon). \tag{25}$$

□

Lemma 3. *The $O(1)$ terms from the momentum equations in Eq. (16) are the semi-discretization of the limiting equation*

$$(\mathbf{v}_{(0)})_t + \frac{\nabla p_{(2)}}{\rho_{(0)}} + \nabla\cdot(\mathbf{v}_{(0)}\otimes\mathbf{v}_{(0)}) = 0, \tag{26}$$

under the assumptions of Lemma 1, with an implicit treatment of pressure term $p_{(2)}$ and an explicit treatment of the tensor product $(\mathbf{v}_{(0)} \otimes \mathbf{v}_{(0)})$.

Proof. Consider the $O(1)$ terms from the momentum equations along with the results from Eq. (24) and Eq. (25) with the stiffness parameter $\varepsilon \to 0$,

$$\begin{aligned}
\rho^{n+1}_{(0)} u^{n+1}_{(0)} &= \rho^{n}_{(0)} u^{n}_{(0)} - \Delta t \partial_x p^{n+1}_{(2)} - \Delta t \rho^{n}_{(0)} \left(\left(u^2_{(0)} \right)_x + \left(u_{(0)} v_{(0)} \right)_y \right)^n - \frac{\Delta t^2}{2} \partial_x \left(\left(p' \left((\rho u)_x + (\rho v)_y \right) \right)_{(2)} \right)^{n+1} \\
&\quad + \frac{\Delta t^2}{2} \rho^{n}_{(0)} \partial_x \left(2 u_{(0)} \left(\left(u^2_{(0)} + \frac{p_{(2)}}{\rho_{(0)}} \right)_x + \left(u_{(0)} v_{(0)} \right)_y \right) \right)^n \\
&\quad + \frac{\Delta t^2}{2} \rho^{n}_{(0)} \partial_y \left(v_{(0)} \left(\left(u^2_{(0)} + \frac{p_{(2)}}{\rho_{(0)}} \right)_x + \left(u_{(0)} v_{(0)} \right)_y \right) + u_{(0)} \left(\left(u_{(0)} v_{(0)} \right)_x + \left(v^2_{(0)} + \frac{p_{(2)}}{\rho_{(0)}} \right)_y \right) \right)^n \\
\rho^{n+1}_{(0)} v^{n+1}_{(0)} &= \rho^{n}_{(0)} v^{n}_{(0)} - \Delta t \partial_y p^{n+1}_{(2)} - \Delta t \rho^{n}_{(0)} \left(\left(u_{(0)} v_{(0)} \right)_x + \left(v^2_{(0)} \right)_y \right)^n - \frac{\Delta t^2}{2} \partial_y \left(\left(p' \left((\rho u)_x + (\rho v)_y \right) \right)_{(2)} \right)^{n+1} \\
&\quad + \frac{\Delta t^2}{2} \rho^{n}_{(0)} \partial_x \left(v_{(0)} \left(\left(u^2_{(0)} + \frac{p_{(2)}}{\rho_{(0)}} \right)_x + \left(u_{(0)} v_{(0)} \right)_y \right) + u_{(0)} \left(\left(u_{(0)} v_{(0)} \right)_x + \left(v^2_{(0)} + \frac{p_{(2)}}{\rho_{(0)}} \right)_y \right) \right)^n \\
&\quad + \frac{\Delta t^2}{2} \rho^{n}_{(0)} \partial_y \left(2 v_{(0)} \left(\left(u_{(0)} v_{(0)} \right)_x + \left(v^2_{(0)} + \frac{p_{(2)}}{\rho_{(0)}} \right)_y \right) \right)^n ,
\end{aligned}$$

where

$$\left(p' \left((\rho u)_x + (\rho v)_y \right) \right)_{(2)} = p'_{(0)} \left((\rho_{(0)} u_{(2)} + \rho_{(2)} u_{(0)})_x + (\rho_{(0)} v_{(2)} + \rho_{(2)} v_{(0)})_y \right).$$

Upon dividing the above equations by the term $\rho_{(0)}$, we get

$$\begin{aligned}
\mathbf{v}^{n+1}_{(0)} = \; & \mathbf{v}^{n}_{(0)} + \Delta t \left\{ \nabla \cdot \left(-\frac{p_{(2)}}{\rho_{(0)}} \mathbf{Id} \right)^{n+1} + \nabla \cdot \left(-\mathbf{v}_{(0)} \otimes \mathbf{v}_{(0)} \right)^n \right\} \\
& + \frac{\Delta t^2}{2} \left\{ \partial_x \left(\mathcal{J}^{(0)}_x \nabla \cdot \left(\mathbf{v}_{(0)} \otimes \mathbf{v}_{(0)} + \frac{p_{(2)}}{\rho_{(0)}} \mathbf{Id} \right) \right)^n + \partial_y \left(\mathcal{J}^{(0)}_y \nabla \cdot \left(\mathbf{v}_{(0)} \otimes \mathbf{v}_{(0)} + \frac{p_{(2)}}{\rho_{(0)}} \mathbf{Id} \right) \right)^n \right. \\
& \left. - \nabla \cdot \left(\frac{p_{(2)}}{\rho_{(0)}} \left(\rho_{(0)} \nabla \cdot \mathbf{v}_{(2)} + \mathbf{v}_{(0)} \cdot \nabla \rho_{(2)} \right) \mathbf{Id} \right)^{n+1} \right\}
\end{aligned} \tag{27}$$

where $\mathcal{J}^{(0)}_x$ and $\mathcal{J}^{(0)}_y$ are the Jacobian matrices given by

$$\mathcal{J}^{(0)}_x = \begin{pmatrix} 2u_{(0)} & 0 \\ v_{(0)} & u_{(0)} \end{pmatrix} \quad \text{and} \quad \mathcal{J}^{(0)}_y = \begin{pmatrix} v_{(0)} & u_{(0)} \\ 0 & 2v_{(0)} \end{pmatrix}. \tag{28}$$

Eq. (27) is nothing but the semi-discretization of the limiting equation (6) using the two-derivative IMEX-Taylor rule (14) when applied to the splitting

$$\begin{pmatrix} u_{(0)} \\ v_{(0)} \end{pmatrix}_t + \nabla \cdot \underbrace{\begin{pmatrix} \frac{p_{(2)}}{\rho_{(0)}} & 0 \\ 0 & \frac{p_{(2)}}{\rho_{(0)}} \end{pmatrix}}_{\mathbf{F}_{\mathrm{I}}(\mathbf{w}_{(0)})} + \nabla \cdot \underbrace{\begin{pmatrix} u^2_{(0)} & u_{(0)} v_{(0)} \\ u_{(0)} v_{(0)} & v^2_{(0)} \end{pmatrix}}_{\mathbf{F}_{\mathrm{E}}(\mathbf{w}_{(0)})} = 0,$$

which can be simplified to

$$\left(\mathbf{v}_{(0)} \right)_t + \frac{\nabla p_{(2)}}{\rho_{(0)}} + \nabla \cdot \left(\mathbf{v}_{(0)} \otimes \mathbf{v}_{(0)} \right) = 0.$$

□

2.2. Fully-discrete asymptotic analysis

Let the spatial domain $\Omega \subset \mathbb{R}^2$ be divided into $\mathcal{N}_E$ non-overlapping mesh elements

$$\Omega = \bigcup_{e=1}^{\mathcal{N}_E} \Omega_e.$$

Let $\mathcal{T}$ denotes the set of all mesh elements Ω_e and $\partial\mathcal{T}$ denotes the set of all element boundaries. In each Ω_e, we define a space of polynomials of degree $\mathcal{N}_p$, denoted by $\Pi_{\mathcal{N}_p}(\Omega_e)$. The space $\Pi_{\mathcal{N}_p}(\Omega_e)$ is constructed by the tensor product of the one-dimensional Lagrange interpolation polynomials of degree $\mathcal{N}_p$. Now, we define the space of broken polynomials $V_{\mathcal{N}_p}$ on the basis of the above spatial discretization by setting

$$V_{\mathcal{N}_p} := \left\{ \nu \in L^2(\Omega) \;\middle|\; \nu|_{\Omega_e} \in \Pi_{\mathcal{N}_p}(\Omega_e)\ \forall e \leq \mathcal{N}_E \right\},$$

and let $V^k_{\mathcal{N}_p}$ denotes the following product space

$$V^k_{\mathcal{N}_p} := \underbrace{V_{\mathcal{N}_p} \times V_{\mathcal{N}_p} \times \cdots \times V_{\mathcal{N}_p}}_{k \text{ times}}.$$

As per the definition, any function in $V^k_{\mathcal{N}_p}$ is allowed to have discontinuities over a cell boundary. Therefore, for any $\mathbf{x} \in \partial\Omega_e$ and the outward pointing normal vector n_e to Ω_e, we define

$$\xi^{\mathrm{R}} := \lim_{\delta \to 0} \xi(\mathbf{x} + |\delta| n_e),$$

as the exterior and

$$\xi^{\mathrm{L}} := \lim_{\delta \to 0} \xi(\mathbf{x} - |\delta| n_e),$$

as the interior values of $\xi(x)$ at $\mathbf{x}$. Finally, we define the following bilinear operators

$$(\mathbf{a}, \mathbf{b})_{\mathcal{T}} : (\mathbf{a}, \mathbf{b}) \in V^k_{\mathcal{N}_p} \times V^k_{\mathcal{N}_p} \to \sum_{e=1}^{\mathcal{N}_E} \int_{\Omega_e} \mathbf{a} \cdot \mathbf{b}\, dx$$

for the integral over whole domain Ω, and

$$\{\mathbf{a}, b\}_{\partial\mathcal{T}} : (\mathbf{a}, b) \in V^k_{\mathcal{N}_p} \times V^1_{\mathcal{N}_p} \to \sum_{e=1}^{\mathcal{N}_E} \int_{\partial\Omega_e} \left(\mathbf{a}^{\mathrm{R}} + \mathbf{a}^{\mathrm{L}}\right) b \cdot \mathbf{n}_e\, ds,$$

$$[\![\mathbf{a}, b]\!]_{\partial\mathcal{T}} : (\mathbf{a}, b) \in V^k_{\mathcal{N}_p} \times V^1_{\mathcal{N}_p} \to \sum_{e=1}^{\mathcal{N}_E} \int_{\partial\Omega_e} \left(\mathbf{a}^{\mathrm{L}} - \mathbf{a}^{\mathrm{R}}\right) b\, ds,$$

for the integral over domain boundaries $\partial\Omega$.

The DGSEM utilizes the weak formulation of Eq. (3). Therefore , at each time step t^n, we search for an approximate solution $\mathbf{w} = (\rho^n, \rho\mathbf{v}^n)$ to the two-dimensional isentropic Euler equations (3) in $V^3_{\mathcal{N}_p}$. The approximation to the first derivative $\mathbf{w}_t$ is given by

$$(\mathbf{w}_t, \phi)_{\mathcal{T}} - (\mathbf{F}(\mathbf{w}), \nabla\phi)_{\mathcal{T}} + \frac{1}{2}\{\mathbf{F}^*(\mathbf{w}), \phi\}_{\partial\mathcal{T}} + \lambda [\![\mathbf{w}, \phi]\!]_{\partial\mathcal{T}},\ \forall\phi \in \Pi_{\mathcal{N}_p}; \tag{29}$$

the second derivative $\mathbf{w}_{tt}$ is given by

$$(\mathbf{w}_{tt}, \phi)_{\mathcal{T}} - \left(\frac{\partial\mathbf{F}(\mathbf{w})}{\partial\mathbf{w}}\boldsymbol{\sigma}, \nabla\phi\right)_{\mathcal{T}} + \frac{1}{2}\left\{\frac{\partial\mathbf{F}^*(\mathbf{w})}{\partial\mathbf{w}}\boldsymbol{\sigma}, \phi\right\}_{\partial\mathcal{T}} + \lambda [\![\boldsymbol{\sigma}, \phi]\!]_{\partial\mathcal{T}},\ \forall\phi \in \Pi_{\mathcal{N}_p}, \tag{30}$$

with the artificial quantity

$$\boldsymbol{\sigma} := \mathbf{R}^{(1)}(\mathbf{w}) \equiv \mathbf{w}_t \tag{31}$$

as introduced in [32]. $\mathbf{F}^*(\mathbf{w})$ is the global Lax-Friedrichs numerical flux that depends on the left ($\mathbf{w}^{\mathrm{L}}$) and right ($\mathbf{w}^{\mathrm{R}}$) states with respect to the cell-edge, and $\boldsymbol{\lambda}$ is a globally constant vector. For isentropic Euler equations, the $\boldsymbol{\lambda}$ values for the explicit and implicit numerical fluxes (corresponding to $\mathbf{F}_{\mathrm{E}}$ and $\mathbf{F}_{\mathrm{I}}$ from Eq. (15)) are chosen to be

$$\boldsymbol{\lambda}_{\mathrm{E}} = (\varepsilon, \varepsilon, \varepsilon), \quad \boldsymbol{\lambda}_{\mathrm{I}} = \left(\frac{1}{\varepsilon^2}, 1, 1\right),$$

respectively. If the full flux $\mathbf{F}$ is used for reference, we choose

$$\boldsymbol{\lambda} = \left(\frac{1}{\varepsilon^2}, 1, 1\right).$$

The particular $\boldsymbol{\lambda}$ values given above are wisely chosen to ensure the asymptotic preserving property of the schemes [39].

For the two-dimensional isentropic Euler equations (15), the the fully discrete two-derivative IMEX-Taylor method (Alg. 1) is given by

$$\begin{aligned}
0 = \left(\mathbf{w}^{n+1} - \mathbf{w}^n, \phi\right)_{\mathcal{T}} + \Delta t \; & \left\{ - \left(\mathbf{F}_{\mathrm{I}}(\mathbf{w}^{n+1}), \nabla\phi\right)_{\mathcal{T}} + \frac{1}{2}\left\{\mathbf{F}_{\mathrm{I}}(\mathbf{w}^{n+1}), \phi\right\}_{\partial\mathcal{T}} + \frac{1}{2}\,\mathrm{Diag}\left[\frac{1}{\varepsilon^2}, 1, 1\right]\left[\!\left[\mathbf{w}^{n+1}, \phi\right]\!\right]_{\partial\mathcal{T}} \right\} \\
& + \Delta t \left\{ - \left(\mathbf{F}_{\mathrm{E}}(\mathbf{w}^n), \nabla\phi\right)_{\mathcal{T}} + \frac{1}{2}\left\{\mathbf{F}_{\mathrm{E}}(\mathbf{w}^n), \phi\right\}_{\partial\mathcal{T}} + \varepsilon\left[\!\left[\mathbf{w}^n, \phi\right]\!\right]_{\partial\mathcal{T}} \right\} \\
& - \frac{\Delta t^2}{2} \left\{ - \left(\frac{\partial \mathbf{F}_{\mathrm{I}}(\mathbf{w}^{n+1})}{\partial \mathbf{w}} \boldsymbol{\sigma}^{n+1}, \nabla\phi\right)_{\mathcal{T}} + \frac{1}{2}\left\{\frac{\partial \mathbf{F}_{\mathrm{I}}(\mathbf{w}^{n+1})}{\partial \mathbf{w}} \boldsymbol{\sigma}^{n+1}, \phi\right\}_{\partial\mathcal{T}} + \frac{1}{2}\,\mathrm{Diag}\left[\frac{1}{\varepsilon^2}, 1, 1\right]\left[\!\left[\boldsymbol{\sigma}^{n+1}, \phi\right]\!\right]_{\partial\mathcal{T}} \right\} \\
& + \frac{\Delta t^2}{2} \left\{ - \left(\frac{\partial \mathbf{F}_{\mathrm{E}}(\mathbf{w}^n)}{\partial \mathbf{w}} \mathbf{R}^{(1)}(\mathbf{w}^n), \nabla\phi\right)_{\mathcal{T}} + \frac{1}{2}\left\{\frac{\partial \mathbf{F}_{\mathrm{E}}(\mathbf{w}^n)}{\partial \mathbf{w}} \mathbf{R}^{(1)}(\mathbf{w}^n), \phi\right\}_{\partial\mathcal{T}} + \varepsilon\left[\!\left[\mathbf{R}^{(1)}(\mathbf{w}^n), \phi\right]\!\right]_{\partial\mathcal{T}} \right\}.
\end{aligned} \tag{32}$$

We solve the above expression (32) for $\mathbf{w}^{n+1}$ along with a discretization of (31), given by

$$\begin{aligned}
0 = \left(\boldsymbol{\sigma}^{n+1}, \phi\right)_{\mathcal{T}} & - \left(\mathbf{F}_{\mathrm{I}}(\mathbf{w}^{n+1}), \nabla\phi\right)_{\mathcal{T}} + \frac{1}{2}\left\{\mathbf{F}_{\mathrm{I}}(\mathbf{w}^{n+1}), \phi\right\}_{\partial\mathcal{T}} + \frac{1}{2}\,\mathrm{Diag}\left[\frac{1}{\varepsilon^2}, 1, 1\right]\left[\!\left[\mathbf{w}^{n+1}, \phi\right]\!\right]_{\partial\mathcal{T}} \\
& - \left(\mathbf{F}_{\mathrm{E}}(\mathbf{w}^n), \nabla\phi\right)_{\mathcal{T}} + \frac{1}{2}\left\{\mathbf{F}_{\mathrm{E}}(\mathbf{w}^n), \phi\right\}_{\partial\mathcal{T}} + \varepsilon\left[\!\left[\mathbf{w}^n, \phi\right]\!\right]_{\partial\mathcal{T}}
\end{aligned} \tag{33}$$

Consider the asymptotic expansion of the numerical solution

$$\mathbf{w}^{n+1} = \mathbf{w}^{n+1}_{(0)} + \varepsilon\mathbf{w}^{n+1}_{(1)} + \varepsilon^2\mathbf{w}^{n+1}_{(2)} + O(\varepsilon^3) \quad \text{and} \quad \boldsymbol{\sigma}^{n+1} = \boldsymbol{\sigma}^{n+1}_{(0)} + \varepsilon\boldsymbol{\sigma}^{n+1}_{(1)} + \varepsilon^2\boldsymbol{\sigma}^{n+1}_{(2)} + O(\varepsilon^3),$$

with $\boldsymbol{\sigma} = \left(\boldsymbol{\sigma}_\rho, \boldsymbol{\sigma}_{\rho u}, \boldsymbol{\sigma}_{\rho v}\right)^T =: \left(\boldsymbol{\sigma}_\rho, \boldsymbol{\sigma}_{\rho \mathbf{v}}\right)^T$.

Theorem 2. *The two-derivative IMEX-Taylor method combined with the DeTa splitting* (15) *and spatially discretized with DGSEM is asymptotically consistent, in the sense that the formal limit* $\varepsilon \to 0$ *of the numerical solution* (32)(33) *with well-prepared initial data and periodic boundary conditions, is a consistent discretization of the incompressible Euler equations* (6).

Proof. The proof of the theorem follows from Lemmas 4 , 5 and 6, which show the well preparedness of the updated solution. Lemmas 7 and 8 shows that the limiting method is a consistent discretization of the limiting equations. □

Expanding the components of the $\boldsymbol{\sigma}$ equations, we get

$$0 = \left(\boldsymbol{\sigma}_{\rho}^{n+1}, \phi\right)_{\mathcal{T}} - \left(\rho^{n+1}\mathbf{v}^{n+1}, \nabla\phi\right)_{\mathcal{T}} + \frac{1}{2}\left\{\rho^{n+1}\mathbf{v}^{n+1}, \phi\right\}_{\partial\mathcal{T}} + \frac{1}{2\varepsilon^2}\left[\!\left[\rho^{n+1}, \phi\right]\!\right]_{\partial\mathcal{T}} + \varepsilon\left[\!\left[\rho^{n}, \phi\right]\!\right]_{\partial\mathcal{T}}, \tag{34}$$

$$\begin{aligned} 0 = \left(\boldsymbol{\sigma}_{\rho\mathbf{v}}^{n+1}, \phi\right)_{\mathcal{T}} &- \left(\frac{1-\varepsilon^2}{\varepsilon^2}p^{n+1}\mathbf{Id}, \nabla\phi\right)_{\mathcal{T}} + \frac{1}{2}\left\{\frac{1-\varepsilon^2}{\varepsilon^2}p^{n+1}\mathbf{Id}, \phi\right\}_{\partial\mathcal{T}} + \left[\!\left[\rho^{n+1}\mathbf{v}^{n+1}, \phi\right]\!\right]_{\partial\mathcal{T}} \\ &- \left((\rho\mathbf{v}\otimes\mathbf{v} + p\mathbf{Id})^{n}, \nabla\phi\right)_{\mathcal{T}} + \frac{1}{2}\left\{(\rho\mathbf{v}\otimes\mathbf{v} + p\mathbf{Id})^{n}, \phi\right\}_{\partial\mathcal{T}} + \varepsilon\left[\!\left[\rho^{n}\mathbf{v}^{n}, \phi\right]\!\right]_{\partial\mathcal{T}}. \end{aligned} \tag{35}$$

Lemma 4. *The quantities $\rho_{(0)}^{n+1}$ and $\rho_{(1)}^{n+1}$ in the asymptotic expansion of ρ^{n+1} are continuous across the entire spatial domain under the assumptions of Theorem 2.*

Proof. The $O(\varepsilon^{-2})$ and $O(\varepsilon^{-1})$ terms from Eq. (34) give

$$\left[\!\left[\rho_{(0)}^{n+1}, \phi\right]\!\right]_{\partial\mathcal{T}} = 0, \quad \text{and} \quad \left[\!\left[\rho_{(1)}^{n+1}, \phi\right]\!\right]_{\partial\mathcal{T}} = 0. \tag{36}$$

[33, Lemma 2] applied to Eq. (36) implies the continuity of $\rho_{(0)}^{n+1}$ and $\rho_{(1)}^{n+1}$ over the entire spatial domain. □

Lemma 5. *The quantities $\rho_{(0)}^{n+1}$ and $\rho_{(1)}^{n+1}$ in the asymptotic expansion of ρ^{n+1} are constant in space under the assumptions of Theorem 2.*

Proof. The $O(\varepsilon^{-2})$ and $O(\varepsilon^{-1})$ terms from Eq. (35) give

$$\begin{aligned} -\left(p_{(0)}^{n+1}\mathbf{Id}, \nabla\phi\right)_{\mathcal{T}} + \frac{1}{2}\left\{p_{(0)}^{n+1}\mathbf{Id}, \phi\right\}_{\partial\mathcal{T}} = 0, \\ -\left(p_{(1)}^{n+1}\mathbf{Id}, \nabla\phi\right)_{\mathcal{T}} + \frac{1}{2}\left\{p_{(1)}^{n+1}\mathbf{Id}, \phi\right\}_{\partial\mathcal{T}} = 0. \end{aligned}$$

Applying integration by parts to the above equations with the continuity results from Lemma 4 gives

$$\begin{aligned} \left(\nabla\cdot p_{(0)}^{n+1}\mathbf{Id}, \phi\right)_{\mathcal{T}} + \frac{1}{2}\left[\!\left[p_{(0)}^{n+1}\mathbf{Id}\cdot n_e, \phi\right]\!\right]_{\partial\mathcal{T}} = 0 \quad &\Rightarrow \left(\nabla p_{(0)}^{n+1}, \phi\right)_{\mathcal{T}} = 0, \\ \left(\nabla\cdot p_{(1)}^{n+1}\mathbf{Id}, \phi\right)_{\mathcal{T}} + \frac{1}{2}\left[\!\left[p_{(1)}^{n+1}\mathbf{Id}\cdot n_e, \phi\right]\!\right]_{\partial\mathcal{T}} = 0 \quad &\Rightarrow \left(\nabla p_{(1)}^{n+1}, \phi\right)_{\mathcal{T}} = 0. \end{aligned}$$

Choosing $\phi = \partial_{x_d} p_{(m)}^{n+1}$ ($m \in \{0, 1\}$), the partial derivative with respect to the variable x_d and substituting in the above equations result

$$\left(\nabla p_{(m)}^{n+1}, \partial_{x_d} p_{(m)}^{n+1}\right)_{\mathcal{T}} = 0 \quad \Rightarrow \partial_{x_d} p_{(m)}^{n+1} = 0, \ \forall m \in \{0, 1\} \text{ and } \forall d.$$

Hence, the quantities $\rho_{(0)}^{n+1}$ and $\rho_{(1)}^{n+1}$ are constant in space. □

Consider the density equation from Eq. (32)

$$\begin{aligned} 0 = \left(\rho^{n+1} - \rho^{n}, \phi\right)_{\mathcal{T}} + \Delta t\left\{-\left(\rho^{n+1}\mathbf{v}^{n+1}, \nabla\phi\right)_{\mathcal{T}} + \frac{1}{2}\left\{\rho^{n+1}\mathbf{v}^{n+1}, \phi\right\}_{\partial\mathcal{T}} + \frac{1}{2\varepsilon^2}\left[\!\left[\rho^{n+1}, \phi\right]\!\right]_{\partial\mathcal{T}}\right\} \\ -\frac{\Delta t^2}{2}\left\{-\left(\boldsymbol{\sigma}_{\rho\mathbf{v}}^{n+1}, \nabla\phi\right)_{\mathcal{T}} + \frac{1}{2}\left\{\boldsymbol{\sigma}_{\rho\mathbf{v}}^{n+1}, \phi\right\}_{\partial\mathcal{T}} + \frac{1}{2\varepsilon^2}\left[\!\left[\boldsymbol{\sigma}_{\rho}^{n+1}, \phi\right]\!\right]_{\partial\mathcal{T}}\right\}. \end{aligned} \tag{37}$$

Lemma 6. *The quantities $\rho_{(0)}^{n+1}$ and $\rho_{(1)}^{n+1}$ in the asymptotic expansion of ρ^{n+1} are constant in time under the assumptions of Theorem 2.*

Proof. The $O(1)$ terms from density equation (37) are

$$\begin{aligned} 0 = \left(\rho_{(0)}^{n+1} - \rho_{(0)}^{n}, \phi\right)_{\mathcal{T}} + \Delta t\left\{-\left(\rho_{(0)}^{n+1}\mathbf{v}_{(0)}^{n+1}, \nabla\phi\right)_{\mathcal{T}} + \frac{1}{2}\left\{\rho_{(0)}^{n+1}\mathbf{v}_{(0)}^{n+1}, \phi\right\}_{\partial\mathcal{T}} + \frac{1}{2}\left[\!\left[\rho_{(2)}^{n+1}, \phi\right]\!\right]_{\partial\mathcal{T}}\right\} \\ -\frac{\Delta t^2}{2}\left\{-\left(\boldsymbol{\sigma}_{\rho\mathbf{v}(0)}^{n+1}, \nabla\phi\right)_{\mathcal{T}} + \frac{1}{2}\left\{\boldsymbol{\sigma}_{\rho\mathbf{v}(0)}^{n+1}, \phi\right\}_{\partial\mathcal{T}} + \frac{1}{2}\left[\!\left[\boldsymbol{\sigma}_{\rho(2)}^{n+1}, \phi\right]\!\right]_{\partial\mathcal{T}}\right\}. \end{aligned}$$

Substituting $\phi \equiv 1$ in the above equation, we get

$$0 = \left(\rho_{(0)}^{n+1} - \rho_{(0)}^{n}, 1\right)_{\mathcal{T}} + \Delta t \left\{ \frac{1}{2} \left\{ \rho_{(0)}^{n+1} \mathbf{v}_{(0)}^{n+1}, 1 \right\}_{\partial\mathcal{T}} + \frac{1}{2} \left[\!\left[\rho_{(2)}^{n+1}, 1 \right]\!\right]_{\partial\mathcal{T}} \right\} - \frac{\Delta t^2}{2} \left\{ \frac{1}{2} \left\{ \boldsymbol{\sigma}_{\rho\mathbf{v}(0)}^{n+1}, 1 \right\}_{\partial\mathcal{T}} + \frac{1}{2} \left[\!\left[\boldsymbol{\sigma}_{\rho(2)}^{n+1}, 1 \right]\!\right]_{\partial\mathcal{T}} \right\}.$$

As we assume periodic boundary conditions, the boundary integrals will add up to zero. Combining the result from Lemma 5, we obtain

$$\left(\rho_{(0)}^{n+1} - \rho_{(0)}^{n}\right)(1,1)_{\mathcal{T}} = 0 \quad \Rightarrow \rho_{(0)}^{n+1} - \rho_{(0)}^{n} = 0.$$

Similarly, it can be shown that $\rho_{(1)}^{n+1} - \rho_{(1)}^{n} = 0$, using $O(\varepsilon)$ terms from density equation (37). Therefore, the quantities $\rho_{(0)}^{n+1}$ and $\rho_{(1)}^{n+1}$ are constant in space and time. □

Lemma 7. *The $O(1)$ terms from the density equation (37) form a consistent discretization of $\nabla \cdot \mathbf{v}_{(0)} = 0$ under the assumptions of Theorem 2.*

Proof. Consider the $O(1)$ terms from the density equation (37) with the results from Lemmas 5 and 6

$$\begin{aligned} 0 = \Delta t \Bigg\{ &- \left(\mathbf{v}_{(0)}^{n+1}, \nabla\phi\right)_{\mathcal{T}} + \frac{1}{2} \left\{ \mathbf{v}_{(0)}^{n+1}, \phi \right\}_{\partial\mathcal{T}} + \frac{1}{2} \left[\!\left[\frac{\rho_{(2)}^{n+1}}{\rho_{(0)}}, \phi \right]\!\right]_{\partial\mathcal{T}} \Bigg\} \\ &- \frac{\Delta t^2}{2} \left\{ - \left(\frac{\boldsymbol{\sigma}_{\rho\mathbf{v}(0)}^{n+1}}{\rho_{(0)}}, \nabla\phi \right)_{\mathcal{T}} + \frac{1}{2} \left\{ \frac{\boldsymbol{\sigma}_{\rho\mathbf{v}(0)}^{n+1}}{\rho_{(0)}}, \phi \right\}_{\partial\mathcal{T}} + \frac{1}{2} \left[\!\left[\frac{\boldsymbol{\sigma}_{\rho(2)}^{n+1}}{\rho_{(0)}}, \phi \right]\!\right]_{\partial\mathcal{T}} \right\}. \end{aligned}$$

The above equation is nothing but the implicit two-derivative DGSEM discretization of $\nabla \cdot \mathbf{v}_{(0)}$ along with the $O(1)$ terms from Eqs. (34) and (35). □

Reconsider the momentum equations from Eq. (32),

$$\begin{aligned} 0 = \left(\rho^{n+1}\mathbf{v}^{n+1} - \rho^{n}\mathbf{v}^{n}, \phi\right)_{\mathcal{T}} &+ \Delta t \left\{ - \left(\frac{1-\varepsilon^2}{\varepsilon^2} p^{n+1} \mathbf{Id}, \nabla\phi \right)_{\mathcal{T}} + \frac{1}{2} \left\{ \frac{1-\varepsilon^2}{\varepsilon^2} p^{n+1} \mathbf{Id}, \phi \right\}_{\partial\mathcal{T}} + \frac{1}{2} \left[\!\left[\rho^{n+1}\mathbf{v}^{n+1}, \phi \right]\!\right]_{\partial\mathcal{T}} \right\} \\ &+ \Delta t \left\{ - \left((\rho\mathbf{v}\otimes\mathbf{v} + p\mathbf{Id})^{n}, \nabla\phi \right)_{\mathcal{T}} + \frac{1}{2} \left\{ (\rho\mathbf{v}\otimes\mathbf{v} + p\mathbf{Id})^{n}, \phi \right\}_{\partial\mathcal{T}} + \varepsilon \left[\!\left[\rho^{n}\mathbf{v}^{n}, \phi \right]\!\right]_{\partial\mathcal{T}} \right\} \\ &- \frac{\Delta t^2}{2} \left\{ - \left(\frac{1-\varepsilon^2}{\varepsilon^2} p'^{n+1} \boldsymbol{\sigma}_{\rho}^{n+1} \mathbf{Id}, \nabla\phi \right)_{\mathcal{T}} + \frac{1}{2} \left\{ \frac{1-\varepsilon^2}{\varepsilon^2} p'^{n+1} \boldsymbol{\sigma}_{\rho}^{n+1} \mathbf{Id}, \phi \right\}_{\partial\mathcal{T}} + \frac{1}{2} \left[\!\left[\boldsymbol{\sigma}_{\rho\mathbf{v}}^{n+1}, \phi \right]\!\right]_{\partial\mathcal{T}} \right\} \\ &+ \frac{\Delta t^2}{2} \left\{ - \left((p'\mathbf{Id} - \mathbf{v}\otimes\mathbf{v})^{n} \mathbf{R}_{\rho}^{(1)}(\mathbf{w}^{n}) + \rho\mathcal{J}\cdot\mathbf{R}_{\rho\mathbf{v}}^{(1)}(\mathbf{w}^{n}), \nabla\phi \right)_{\mathcal{T}} \right. \\ &\left. + \frac{1}{2} \left\{ (p'\mathbf{Id} - \mathbf{v}\otimes\mathbf{v})^{n} \mathbf{R}_{\rho}^{(1)}(\mathbf{w}^{n}) + \rho\mathcal{J}\cdot\mathbf{R}_{\rho\mathbf{v}}^{(1)}(\mathbf{w}^{n}), \nabla\phi \right\}_{\partial\mathcal{T}} + \varepsilon \left[\!\left[\boldsymbol{\sigma}_{\rho\mathbf{v}}^{n}, \phi \right]\!\right]_{\partial\mathcal{T}} \right\}, \end{aligned} \tag{38}$$

where $\mathcal{J} = \left[\mathcal{J}_x \,\middle|\, \mathcal{J}_y \right]$ is given by (compare with (28))

$$\mathcal{J}_x = \begin{pmatrix} 2u & 0 \\ v & u \end{pmatrix} \quad \text{and} \quad \mathcal{J}_y = \begin{pmatrix} v & u \\ 0 & 2v \end{pmatrix}.$$

Lemma 8. *The $O(1)$ terms from the momentum equations in Eq. (38) are the two-derivative IMEX-Taylor DGSEM discretization of the limiting equation*

$$\left(\mathbf{v}_{(0)}\right)_t + \frac{\nabla p_{(2)}}{\rho_{(0)}} + \nabla\cdot\left(\mathbf{v}_{(0)}\otimes\mathbf{v}_{(0)}\right) = 0, \tag{39}$$

under the assumptions of Lemmas 5 and 6, with an implicit treatment of pressure term $p_{(2)}$ and an explicit treatment of the tensor product $(\mathbf{v}_{(0)}\otimes\mathbf{v}_{(0)})$.

Proof. Consider the $O(1)$ terms from the momentum equations in Eq. (38) along with results from Lemmas 5 and 6, and applying integration by parts to the explicit pressure term gives

$$\begin{aligned}
0 = \left(\mathbf{v}_{(0)}^{n+1} - \mathbf{v}_{(0)}^{n}, \phi\right)_{\mathcal{T}} &+ \Delta t \left\{ -\left(\frac{p_{(2)}^{n+1}}{\rho_{(0)}}\mathbf{Id}, \nabla\phi\right)_{\mathcal{T}} + \frac{1}{2}\left\{\frac{p_{(2)}^{n+1}}{\rho_{(0)}}\mathbf{Id}, \phi\right\}_{\partial\mathcal{T}} + \frac{1}{2}\left[\!\left[\mathbf{v}_{(0)}^{n+1}, \phi\right]\!\right]_{\partial\mathcal{T}} \right\} \\
&+\Delta t \left\{ -\left(\mathbf{v}_{(0)}^{n} \otimes \mathbf{v}_{(0)}^{n}, \nabla\phi\right)_{\mathcal{T}} + \frac{1}{2}\left\{\mathbf{v}_{(0)}^{n} \otimes \mathbf{v}_{(0)}^{n}, \phi\right\}_{\partial\mathcal{T}} \right\} \\
&-\frac{\Delta t^2}{2} \left\{ -\left(\frac{{p'_{(2)}}^{n+1}}{\rho_{(0)}}\boldsymbol{\sigma}_{\rho(0)}^{n+1}\mathbf{Id}, \nabla\phi\right)_{\mathcal{T}} + \frac{1}{2}\left\{\frac{{p'_{(2)}}^{n+1}}{\rho_{(0)}}\boldsymbol{\sigma}_{\rho(0)}^{n+1}\mathbf{Id}, \phi\right\}_{\partial\mathcal{T}} + \frac{1}{2}\left[\!\left[\frac{\boldsymbol{\sigma}_{\rho\mathbf{v}(0)}^{n+1}}{\rho_{(0)}}, \phi\right]\!\right]_{\partial\mathcal{T}} \right\} \\
&+\frac{\Delta t^2}{2} \left\{ -\left(\mathcal{J}_{(0)} \cdot \mathbf{R}_{\rho\mathbf{v}(0)}^{(1)}(\mathbf{w}^n), \nabla\phi\right)_{\mathcal{T}} + \frac{1}{2}\left\{\mathcal{J}_{(0)} \cdot \mathbf{R}_{\rho\mathbf{v}(0)}^{(1)}(\mathbf{w}^n), \nabla\phi\right\}_{\partial\mathcal{T}} \right\},
\end{aligned}$$

where $\boldsymbol{\sigma}_{\rho(0)}$ and $\boldsymbol{\sigma}_{\rho\mathbf{v}(0)}$ are the respective $O(1)$ terms from Eqs. (34) and (35). The above equation is nothing but the two-derivative IMEX-Taylor DGSEM discretization of the limiting equation (6) when applied to the following splitting

$$\begin{pmatrix} u_{(0)} \\ v_{(0)} \end{pmatrix}_t + \nabla \cdot \underbrace{\begin{pmatrix} \frac{p_{(2)}}{\rho_{(0)}} & 0 \\ 0 & \frac{p_{(2)}}{\rho_{(0)}} \end{pmatrix}}_{\mathbf{F}_{\mathrm{I}}(\mathbf{w}_{(0)})} + \nabla \cdot \underbrace{\begin{pmatrix} u_{(0)}^2 & u_{(0)}v_{(0)} \\ u_{(0)}v_{(0)} & v_{(0)}^2 \end{pmatrix}}_{\mathbf{F}_{\mathrm{E}}(\mathbf{w}_{(0)})} = 0.$$

□

3. Extension to higher order methods

The two-derivative IMEX-Taylor method (14) discussed previously gives a second-order accurate solution. When higher-order implicit or explicit Runge-Kutta methods are concerned, devising them involves a cumbersome process of solving many equations. The number of unknowns and equations exponentially increases as we search for Runge-Kutta schemes with higher orders of accuracy. Due to additional conditions, the scenario worsens when probing for higher-order IMEX schemes. The use of predictor-corrector schemes [15, 18, 19, 27] discussed in the introduction helps overcome the drawbacks of the Runge-Kutta methods mentioned above. The schemes are devised in such a way that the order is increased in each correction step until it hits its maximum achievable order.

Extending implicit predictor-corrector schemes to IMEX schemes is trouble-free. An IMEX predictor step instead of an implicit predictor can change the overall scheme to an IMEX method with slight modifications on the correction steps. Hence, we have the two-derivative IMEX-HBPC scheme given in Alg. 2, which uses the two-derivative IMEX-Taylor scheme as the prediction step. We consider the serial IMEX version of the HBPC algorithm described in [15, 18] incorporating the stability parameters (θ_1, θ_2) introduced in [19].

Algorithm 2 (HBPC$(q, k_{\max})$)**.** *To advance the solution in time, we compute values* $\mathbf{w}^{n,[k],l}$*. To account for the initial conditions* $\mathbf{w}_0 \equiv \mathbf{w}(t=0)$*, define*

$$\mathbf{w}^{-1,[k],s} := \mathbf{w}_0.$$

1. ***Predict.*** *Solve the following expression for* $\mathbf{w}^{n,[0],l}$ *and each* $1 \le l \le s$*:*

$$\mathbf{w}^{n,[0],l} := \mathbf{w}^n + c_l\Delta t\left(\mathbf{R}_I^{(1)}(\mathbf{w}^{n,[0],l}) + \mathbf{R}_E^{(1)}(\mathbf{w}^n)\right) + \frac{(c_l\Delta t)^2}{2}\left(\mathbf{R}_E^{(2)}(\mathbf{w}^n) - \mathbf{R}_I^{(2)}(\mathbf{w}^n, \mathbf{w}^{n,[0],l})\right). \tag{40}$$

2. ***Correct.*** *Next, the corrected values* $\mathbf{w}^{n,[k],l}$ *for* $1 \le k \le k_{\max}$ *are computed through solving for each* $1 \le l \le s$ *and each* $1 \le k \le k_{\max}$*:*

$$\begin{aligned}
\mathbf{w}^{n,[k],l} := \mathbf{w}^n &+ \Delta t\theta_1\left(\mathbf{R}_I^{(1)}(\mathbf{w}^{n,[k],l}) - \mathbf{R}_I^{(1)}(\mathbf{w}^{n,[k-1],l})\right) \\
&- \frac{\Delta t^2}{2}\theta_2\left(\mathbf{R}_I^{(2)}(\mathbf{w}^{n,[k-1],l}, \mathbf{w}^{n,[k],l}) - \mathbf{R}_I^{(2)}(\mathbf{w}^{n,[k-1],l})\right) + \mathcal{I}_l,
\end{aligned} \tag{41}$$

with

$$\mathcal{I}_l := \mathcal{I}_l\left(\mathbf{w}^{n,[k-1],1}, \ldots, \mathbf{w}^{n,[k-1],s}\right). \tag{42}$$

$\mathcal{I}_l(\cdot)$ denotes the q-th order Hermite-Birkhoff quadrature rule.

3. ***Update.*** *In order to retain a first-same-as-last property, we update the solution with*

$$\mathbf{w}^{n+1} := \mathbf{w}^{n,[k_{\max}],s}. \tag{43}$$

Theorem 3. *The two-derivative IMEX-HBPC scheme combined with the DeTa splitting (15) and spatially discretized with DGSEM is asymptotically consistent in the sense that the formal limit $\varepsilon \to 0$ of the numerical solution using Alg. (2) with well-prepared initial data and periodic boundary conditions, is a consistent discretization of the incompressible Euler equations (6).*

Proof. The proof of the asymptotic consistency for the predictor step of the IMEX-HBPC scheme follows the same steps as of Theorem 2. Similar arguments can be extended to the corrector steps to complete the proof. □

4. Solving the (non-)linear system of equations

We use Newton's method to solve the non-linear equations arising in the implicit formulations of the IMEX-HBPC scheme. For a given system of non-linear equations $\mathcal{G}(X) := 0$, Newton's method starts with an initial guess X^0. Then, the following linear equation is solved for the Newton increment ΔX:

$$\frac{\partial \mathcal{G}(X^r)}{\partial X} \cdot \Delta X = -\mathcal{G}(X^r),$$

ΔX is hence used to update the new iterate through

$$X^{r+1} = X^r + \Delta X.$$

The iterative procedure is continued until a desired solution is found that satisfies the imposed stopping criterion. The formulations of the non-linear equations associated with each implicit step of Alg. 1 and Alg. 2 are given by

$$\mathcal{G}(X) \equiv \begin{pmatrix} \mathcal{G}^w(X) \\ \mathcal{G}^\sigma(X) \end{pmatrix} := \begin{pmatrix} \mathbf{w} - \alpha_1 \Delta t \mathbf{R}_{\mathrm{I}}^{(1)}(\mathbf{w}) + \frac{\alpha_2 \Delta t^2}{2} \mathbf{R}_{\mathrm{I}}^{(2)}(\mathbf{w}, \boldsymbol{\sigma}) \\ \boldsymbol{\sigma} - \mathbf{R}_{\mathrm{I}}^{(1)}(\mathbf{w}) \end{pmatrix} - \begin{pmatrix} b(\bar{\mathbf{w}}) \\ \mathbf{R}_{\mathrm{E}}^{(1)}(\bar{\mathbf{w}}) \end{pmatrix} = 0,$$

where $b(\bar{\mathbf{w}})$ and the parameters α_1 and α_2 depend on the respective schemes. The unknown value is denoted as $\mathbf{w}$, whereas $\bar{\mathbf{w}}$ is the known solution from a previous step. The associated Jacobian for the above non-linear equation system is

$$\mathcal{J}(X) := \begin{pmatrix} \mathbf{Id} - \alpha_1 \Delta t \frac{\partial \mathbf{R}_{\mathrm{I}}^{(1)}(\mathbf{w})}{\partial \mathbf{w}} + \frac{\alpha_2 \Delta t^2}{2} \frac{\partial \mathbf{R}_{\mathrm{I}}^{(2)}(\mathbf{w}, \boldsymbol{\sigma})}{\partial \mathbf{w}} & \frac{\alpha_2 \Delta t^2}{2} \frac{\partial \mathbf{R}_{\mathrm{I}}^{(1)}(\mathbf{w})}{\partial \mathbf{w}} \\ -\frac{\partial \mathbf{R}_{\mathrm{I}}^{(1)}(\mathbf{w})}{\partial \mathbf{w}} & \mathbf{Id} \end{pmatrix}. \tag{44}$$

There holds $\frac{\partial \mathbf{R}_{\mathrm{I}}^{(2)}(\mathbf{w},\boldsymbol{\sigma})}{\partial \boldsymbol{\sigma}} = \frac{\partial \mathbf{R}_{\mathrm{I}}^{(1)}(\mathbf{w})}{\partial \mathbf{w}}$ due to the structure of the spatial discretization. Hence, the terms $\frac{\partial \mathbf{R}_{\mathrm{I}}^{(2)}(\mathbf{w},\boldsymbol{\sigma})}{\partial \boldsymbol{\sigma}}$ are replaced by $\frac{\partial \mathbf{R}_{\mathrm{I}}^{(1)}(\mathbf{w})}{\partial \mathbf{w}}$ in the Jacobian defined above.

The linear equations arising in the Newton iterations are solved using the GMRES method. As the GMRES method utilizes the matrix-vector products $\mathcal{J}\Delta X$ for the solution search, we use a matrix-free approach, as done in [34, Sec. 4]. Consult the papers [35] and [36] for more details on the matrix-free implementation. Applying the matrix-free approach, then the Jacobian-vector product is

$$\mathcal{J}\Delta X = \begin{pmatrix} \Delta \mathbf{w} - \alpha_1 \Delta t \frac{\mathbf{R}_{\mathrm{I}}^{(1)}(\mathbf{w}+\varepsilon_{FD}^w \Delta \mathbf{w}) - \mathbf{R}_{\mathrm{I}}^{(1)}(\mathbf{w})}{\varepsilon_{FD}^w} + \frac{\alpha_2 \Delta t^2}{2} \frac{\mathbf{R}_{\mathrm{I}}^{(2)}(\mathbf{w}+\varepsilon_{FD}^w \Delta \mathbf{w}, \boldsymbol{\sigma}) - \mathbf{R}_{\mathrm{I}}^{(2)}(\mathbf{w}, \boldsymbol{\sigma})}{\varepsilon_{FD}^w} + \frac{\alpha_2 \Delta t^2}{2} \frac{\mathbf{R}_{\mathrm{I}}^{(1)}(\mathbf{w}+\varepsilon_{FD}^\sigma \Delta \boldsymbol{\sigma}) - \mathbf{R}_{\mathrm{I}}^{(1)}(\mathbf{w})}{\varepsilon_{FD}^\sigma} \\ -\frac{\mathbf{R}_{\mathrm{I}}^{(1)}(\mathbf{w}+\varepsilon_{FD}^w \Delta \mathbf{w}) - \mathbf{R}_{\mathrm{I}}^{(1)}(\mathbf{w})}{\varepsilon_{FD}^w} + \Delta \boldsymbol{\sigma} \end{pmatrix},$$

replacing the derivatives with finite difference approximations. The small parameter $\varepsilon_{FD}^{(\bullet)}$ denotes the following

$$\varepsilon_{FD}^{(\bullet)} := \frac{\sqrt{\varepsilon_{machine}}}{\varepsilon \left\|\Delta(\bullet)\right\|_2},$$

where ε is the reference Mach number, and $\varepsilon_{machine}$ denotes the approximate machine accuracy, see [34]. In fortran, there exists an intrinsic *epsilon* function, which gives approximately $\varepsilon_{machine} \approx 2 \cdot 10^{-16}$.

An appropriate and efficient preconditioner is necessary for the faster convergence of the GMRES method. We use a problem-tailored extended Block-Jacobi preconditioner as used in [34]. Refer to the figures [34, Fig. 2 and Fig. 4] and the section [34, Sec. 3.2.3] for more details on the construction of the extended Block-Jacobi preconditioner. As shown in [34], neglecting the Hessian contribution ($\frac{\partial \mathbf{R}^{(2)}(\mathbf{w})}{\partial \mathbf{w}}$) from the linear equation and preconditioner does not affect the solution from the GMRES method; we also adopted it in this paper.

4.1. Newton stopping criteria

For a given ε_{Newton}, the stopping criterion for the k^{th} Newton iteration is given by

$$\left\|\mathcal{G}^w(X^k)\right\| < \varepsilon_{Newton} \cdot \left\|\mathcal{G}^w(X^0)\right\|,$$

where $\|(\bullet)\|$ is the L_2 norm. The residual norm stagnates in the Newton procedure as the stiffness of the problem increases ($\varepsilon \leq 10^{-2}$). The implicit solver cannot reduce the residual norm beyond a specific value for low values of ε_{Newton}. In order to address this condition and modify the Newton stopping criteria, we use a stagnated residual norm stopping criteria.

Consider the sequence of residual norms $\left\{\left\|\mathcal{G}^w(X^0)\right\|, \left\|\mathcal{G}^w(X^1)\right\|, \left\|\mathcal{G}^w(X^2)\right\|, \ldots, \left\|\mathcal{G}^w(X^k)\right\|\right\}$ in the Newton iteration. For each Newton iteration k, we define a measure of stagnation (**Ms**) using the following

$$\mathbf{Ms}_k = \frac{\left|\left\|\mathcal{G}^w(X^k)\right\| - \left\|\mathcal{G}^w(X^{k-1})\right\|\right|}{\left\|\mathcal{G}^w(X^{k-1})\right\|}.$$

In each Newton iteration, $\mathbf{Ms}_k$ will be computed. If $\mathbf{Ms}_k \leq \mathcal{M}_{ms}$ and $\left\|\mathcal{G}^w(X^k)\right\| \leq \mathcal{M}_\eta$ holds for predefined values $\mathcal{M}_{ms}$ and η, stagnation counter increases by one. When the stagnation counter hits a predefined value $\mathcal{M}_C$, the Newton stops, indicating that the residual was at a stagnated value for atleast $\mathcal{M}_C$ iterations. If the residual norm oscillates along with the stagnation condition, the algorithm chooses Newton solution with minimal residual norm. The values $\mathcal{M}_{ms}$, $\mathcal{M}_\eta$ and $\mathcal{M}_C$ are user-defined; hence, they will be mentioned for the obtained numerical results in the upcoming section.

5. Numerical Results

The aforementioned time-stepping schemes are implemented in the open-source code FLEXI[1], which is developed to solve hyperbolic-parabolic conservation equations in a discontinuous Galerkin setting [37].

5.1. Higher-order traveling vortex (HOTV)

In this section, we cite an explicit solution to the isentropic Euler equations (3) with parameters $\kappa = 2$ and $\gamma = 0.5$ from [38, 39, 40]. The spatial domain under consideration is $\Omega = [0, 1] \times [0, 1]$, with periodic boundary conditions. The initial conditions are

$$\rho(x, 0) = 2 + (500\varepsilon)^2 \cdot \begin{cases} 0.5e^{\frac{2}{\Delta r}}\Delta r - \mathrm{Ei}(\frac{2}{\Delta r}), & \text{for } r < 0.5, \\ 0, & \text{otherwise} \end{cases}$$

[1] www.flexi-project.org, GNU GPL v3.0

$$u(x,0) = \begin{pmatrix}0.5\\0\end{pmatrix} + 500\begin{pmatrix}-x_2+0.5\\x_1-0.5\end{pmatrix}\cdot\begin{cases}e^{\frac{1}{\Delta r}}, & \text{for } r<0.5,\\ 0, & \text{otherwise}\end{cases}$$

where $r := \sqrt{(x_1-0.5)^2+(x_2-0.5)^2}$ and $\Delta r := r^2 - 0.25$. The exponential integral function Ei(x) is given by

$$\mathrm{Ei}(x) := \int_{-\infty}^{x} \frac{e^t}{t} dt,$$

and it is computed using the algorithm given in [41, Sec. 6.3]. The exact solution corresponding to the above given initial conditions is

$$\rho(x,t) = \rho\left(\begin{pmatrix}x_1-0.5t\\x_2\end{pmatrix},0\right), \quad u(x,t) = u\left(\begin{pmatrix}x_1-0.5t\\x_2\end{pmatrix},0\right). \tag{45}$$

5.2. Timestep selection for the IMEX schemes with DGSEM spatial discretization

We use the formulation of the allowable timestep given in [42] for an explicit scheme under the constraints of CFL conditions for discontinuous Galerkin schemes. For the IMEX scheme, it is given by

$$\Delta t = \mathrm{CFL}_{conv} \cdot \frac{\Delta l}{(2\mathcal{N}_p+1)\cdot|\lambda_\mathrm{E}|_{max}}, \tag{46}$$

where CFL_{conv} is the convective CFL value, $|\lambda_\mathrm{E}|_{max}$ is the maximum of the absolute values of the eigenvalues associated with the explicit flux given by

$$\lambda_1 = 0, \quad \lambda_2 = \mathbf{v}\cdot\mathbf{n} \quad \text{and} \quad \lambda_3 = 2\mathbf{v}\cdot\mathbf{n}, \tag{47}$$

and Δl is the characteristic length of the considered mesh element. The convective CFL value is chosen to be $\mathrm{CFL}_{conv} \leq 1$ for stability.

5.3. Comparison of explicitness-preserving and non-explicitness-preserving IMEX schemes

There are two ways to consider the implicit part of the second derivative, as mentioned in Rem. 1. The schemes that use the formulation in Eq. (13) are called *explicitness-preserving*, and those that use Eq. (12) can be termed *non-explicitness-preserving* IMEX schemes. Hence, any two-derivative IMEX schemes can have these two variants. We have only shown the analysis for explicitness-preserving IMEX-Taylor and IMEX-HBPC schemes in the paper. However, we have verified that Theorems 1, 2 and 3 also hold for their non-explicitness-preserving variants.

Explicitness-preserving schemes are more natural as they give more justice to the concept of IMEX splitting. However, we compare the explicitness and non-explicitness-preserving schemes using IMEX-HBPC(4,3) to understand their computational disparities. Regarding the implicit solver, there is a slight difference on the third block of the Jacobian (44), where it is $-\frac{\partial \mathbf{R}^{(1)}(\mathbf{w})}{\partial \mathbf{w}}$ for the non-explicitness-preserving and $-\frac{\partial \mathbf{R}_\mathrm{I}^{(1)}(\mathbf{w})}{\partial \mathbf{w}}$ for the explicitness-preserving scheme. The difference is also adapted in the respective preconditioner.

For the comparison test, the spatial discretization is set to $\mathcal{N}_E = \{16\times16, 24\times24, 32\times32\}$ with $\mathcal{N}_p = 4$. The CFL_{conv} value is fixed at 0.9. The relative tolerances for the Newton and GMRES iterations are chosen to be 10^{-6} and 10^{-2} respectively with values $\mathcal{M}_{ms} = 0.1$, $\mathcal{M}_\eta = 10^{-5}$ and $\mathcal{M}_C = 3$ for the residual norm stagnation criteria. Then the L_2-errors are computed at final time $T_{end} = 0.1$, compared to the explicit solution (45).

In the first column of Fig. 1, the L_2-error is plotted for various values of stiffness parameters ε ranging from 10^{-3} to 10^0. The scheme converges for explicitness-preserving and non-explicitness-preserving schemes without fail for all the values of $\varepsilon \geq 10^{-3}$, and convergence is nearly not to distinguish.

In the third column of Fig. 1, the average number of GMRES iterations per timestep is plotted for various values of stiffness parameters. There is a notable difference in the linear iterations between explicitness-preserving and non-explicitness-preserving schemes utilized per timestep. The non-explicitness-preserving strategy consumes extra GMRES iterations to achieve the same error reduction as the explicitness-preserving strategy. The difference increases as the stiffness of the system increases. The GMRES iteration consumption is directly reflected in the computational time required for the schemes to complete the simulation. Therefore, in the second column of Fig. 1, it can be seen that the non-explicitness-preserving strategy consumed enormous extra time compared to the explicitness-preserving

strategy. These dissimilarities seen above are mainly due to the additional non-linearity and unnecessary function inversions that the non-explicitness-preserving brings into the scheme.

The disparities discussed above and the results shown in Fig. 1 show the importance of choosing the explicitness-preserving strategy for a multi-derivative IMEX scheme. Therefore, we use the explicitness-preserving scheme for the higher-order extensions in the coming sections to obtain the numerical results.

5.4. Numerical results of IMEX-HBPC schemes on HOTV

Tab. 3 shows the L_2-errors of the IMEX-HBPC schemes up to order eight for various stiffness values. The spatial discretization is set to $\mathcal{N}_E = \{16 \times 16\}$. The polynomial degrees $\mathcal{N}_p$ are chosen as 4, 6, and 8 for IMEX-HBPC$(4, k_{\max})$, IMEX-HBPC$(6, k_{\max})$ and IMEX-HBPC$(8, k_{\max})$, respectively. The errors are calculated compared to the explicit solution (45) at the final time $T_{end} = 2$. The relative tolerances for the Newton and GMRES iterations are chosen to be 10^{-6} and 10^{-2}, respectively, with values $\mathcal{M}_{ms} = 0.3$, $\mathcal{M}_\eta = 10^{-5}$ and $\mathcal{M}_C = 1$ for the residual norm stagnation criteria.

The errors are computed for IMEX-HBPC$(4, k_{\max})$ and IMEX-HBPC$(6, k_{\max})$ schemes at a fixed $\mathrm{CFL}_{conv} = 0.9$. The fourth order scheme showcases convergence for all $\varepsilon \geq 10^{-3}$ for a constant corrections step $k_{\max} = 3$. However, the sixth-order scheme mandates more correction steps as the stiffness increases to achieve the desired convergence. The correction steps ranged from $5 \leq k_{\max} \leq 12$ for $10^0 \leq \varepsilon \leq 10^{-3}$. The fourth order scheme is A-stable for all values of $k_{\max}$, and the sixth order scheme is at least $A(89.7°)$-stable for all possible values of $k_{\max}$, see the stability plots in [19, Fig. 3]. The demand for more correction steps for IMEX-HBPC$(6, k_{\max})$ were hence not needed for stability issues, but rather for the mitigation of a decrease in convergence order, as outlined in [15, Fig. 2].

Compared to the IMEX-HBPC$(4, k_{\max})$ and IMEX-HBPC$(6, k_{\max})$ schemes, the eight order scheme IMEX-HBPC $(8, k_{\max})$ has relatively low stability angle for lower values of $k_{\max}$, see [19, Fig. 3]. The scheme is approximately $A(89.4°)$-stable for $k_{\max} = 7$, and the stability angle drops monotonically to approximately 88.65° for $k_{\max} = 15$. Then, the stability angle gradually increases (with oscillations) to 89.4° for $k_{\max} = 50$. The severity of the oscillations decreased as $k_{\max}$ increased. The above-mentioned oscillating stability properties of the IMEX-HBPC$(8, k_{\max})$ scheme have caused difficulty choosing $(\mathrm{CFL}_{conv}, k_{\max})$ combinations for stiffer problems. In Tab. 3, the errors were computed for $\varepsilon \geq 10^{-2}$, and schemes exhibited convergence for the given $(\mathrm{CFL}_{conv}, k_{\max})$ combinations. The result for $\varepsilon = 10^{-3}$ has been skipped due to the high computational costs required.

6. Conclusions and Outlook

In this paper, we have combined the higher-order two-derivative IMEX-HBPC scheme with higher-order discontinuous Galerkin spatial discretization for isentropic Euler equations. The IMEX-HBPC scheme utilized the DeTa flux splitting [29]. The asymptotic analysis has been done for the semi-discrete and fully-discrete formulations of the isentropic Euler equations. The overall scheme is proven to be asymptotic preserving. Numerical results showed that the IMEX schemes are stable under convective CFL conditions independent of ε.

The implicit part of the second derivative flux has been evaluated in two ways: explicitness-preserving (13) and non-explicitness-preserving (12). It has been shown in the comparison test that the explicitness-preserving scheme is more efficient than the non-explicitness-preserving scheme in terms of the consumed linear iterations. The schemes were theoretically proved asymptotically consistent with the appropriate choice of numerical fluxes. Numerical experiments were performed on the high-order traveling vortex (HOTV) (45) with periodic boundary conditions. Results have been shown for IMEX-HBPC schemes up to order eight, see Tab. 3. All the schemes have exhibited a reduction in the error by their order of accuracy for fixed convective CFL conditions, uniformly for all the ε values.

One of the future research directions is to investigate other possible flux splitting options for the isentropic Euler equations. Also, we are interested in studying the IMEX-HBPC schemes for the Navier-Stokes equations. However, as the PDE system becomes more complex and diffusion terms are involved, selecting appropriate flux splitting and numerical fluxes for the Navier-Stokes equations will be cumbersome. Furthermore, for the parallel-in-time HBPC schemes [18], it is interesting to study and conduct asymptotic analysis on their IMEX versions.

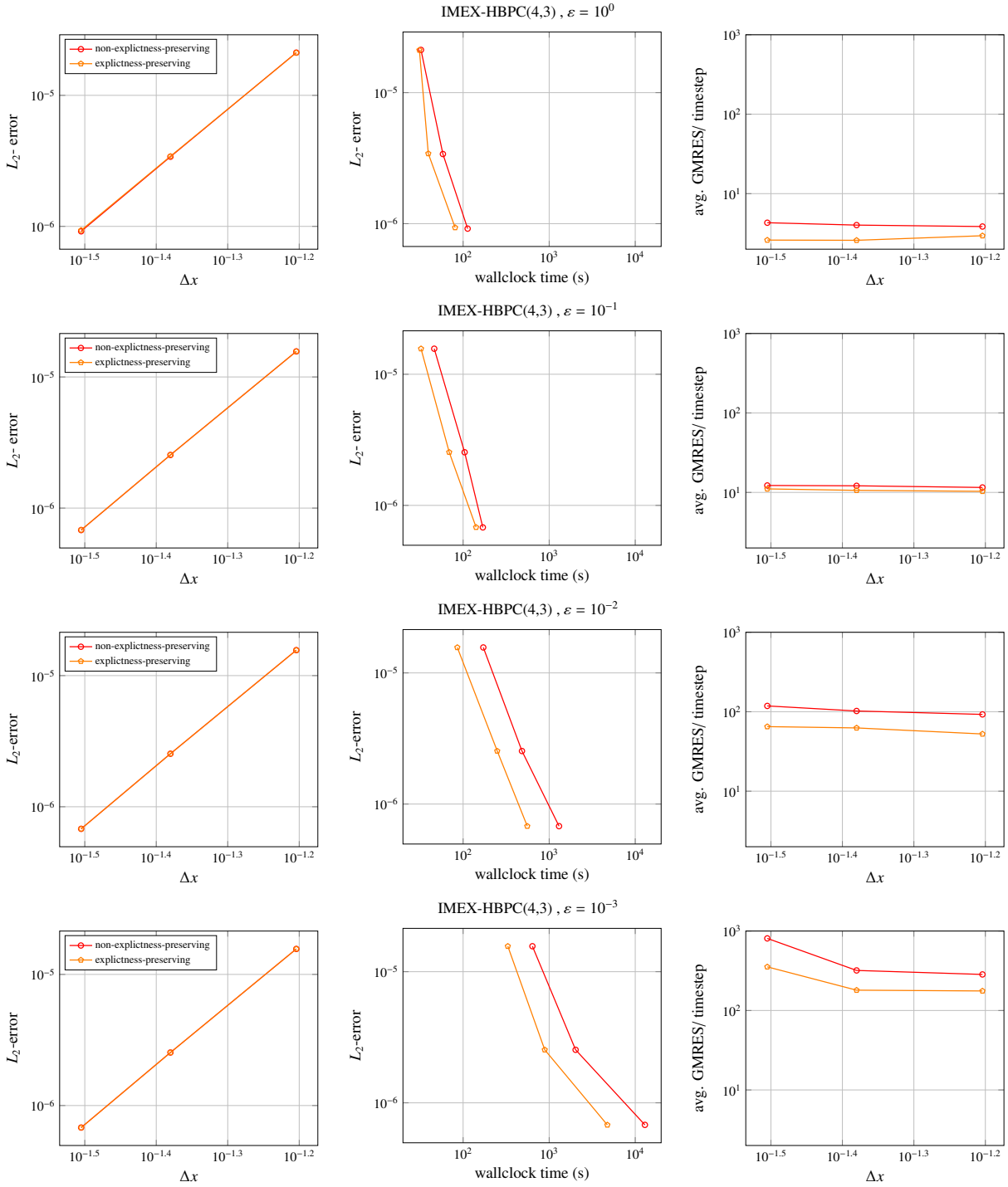

Figure 1. L_2-error vs meshsize (left), L_2-error vs wallclock time (middle), and average number of GMRES iterations per timestep vs meshsize(right) for HOTV Sec. 5.1 with $T_{end} = 0.1$ using IMEX-HBPC43 timestepping scheme plotted for a fixed $\text{CFL}_{conv} = 0.9$. The comparison is made for the strategies *non-explicitness-preserving* and *explicitness-preserving* for different values of stiffness parameter ε. The spatial discretization is set to $\mathcal{N}_E = \{16 \times 16, 24 \times 24, 32 \times 32\}$ with $\mathcal{N}_p = 4$. The Newton and GMRES tolerences are taken to be 10^{-6} and 10^{-2} respectively with in a limit of 50 Newton iterations per implicit solve and 700 GMRES iterations with 50 restarts per Newton iteration. For the residual norm stagnation criteria, the values are chosen to be $\mathcal{M}_{ms} = 0.1$, $\mathcal{M}_\eta = 10^{-5}$ and $\mathcal{M}_C = 3$. The simulations use spatial parallelization on 36 processors.

Scheme	Stiffness(ε)	CFL_{conv}	L_2-error	$k_{\max}$
IMEX-HBPC(4,$k_{\max}$)	10^{-0}	0.9	6.472×10^{-5}	3
	10^{-1}	0.9	5.909×10^{-5}	3
	10^{-2}	0.9	5.895×10^{-5}	3
	10^{-3}	0.9	5.897×10^{-5}	3
IMEX-HBPC(6,$k_{\max}$)	10^{-0}	0.9	1.022×10^{-6}	5
	10^{-1}	0.9	9.857×10^{-7}	7
	10^{-2}	0.9	1.031×10^{-6}	9
	10^{-3}	0.9	9.870×10^{-7}	12
*IMEX-HBPC(8,$k_{\max}$)	10^{-0}	0.9	5.349×10^{-8}	7
	10^{-1}	0.45	3.398×10^{-8}	9
	10^{-2}	0.9	3.382×10^{-8}	50
	10^{-3}	–	–	–

Table 3. Total L_2-error for HOT-vortex at $T_{end} = 2$ for the schemes IMEX-HBPC$(4, k_{\max})$ (top), IMEX-HBPC$(6, k_{\max})$ (middle) and IMEX-HBPC$(8, k_{\max})$ (bottom) for a constant $\text{CFL}_{conv} = 0.9$. *The IMEX-HBPC$(8, k_{\max})$ scheme has used different CFL_{conv} values. The spatial discretization is set to $\mathcal{N}_E = \{16 \times 16\}$ with $\mathcal{N}_p$ equals to 4, 6, and 8 for the schemes IMEX-HBPC$(4, k_{\max})$, IMEX-HBPC$(6, k_{\max})$ and IMEX-HBPC$(8, k_{\max})$, respectively. The Newton and GMRES tolerences are taken to be 10^{-6} and 10^{-2} respectively with in a limit of 50 Newton iterations per implicit solve and 700 GMRES iterations with 50 restarts per Newton iteration. For the residual norm stagnation criteria, the values are chosen to be $\mathcal{M}_{ms} = 0.3$, $\mathcal{M}_\eta = 10^{-5}$ and $\mathcal{M}_C = 1$. The simulations use spatial parallelization on 72 processors.

Acknowledgments

Arjun Thenery Manikantan was funded by the "Bijzonder Onderzoeksfonds" (BOF) from UHasselt - project no. BOF21KP12. We acknowledge the VSC (Flemish Supercomputer Center) for providing computing resources. The VSC is funded by the Research Foundation - Flanders (FWO) and the Flemish Government.

References

[1] R. Courant, K. Friedrichs, H. Lewy, Über die partiellen Differenzengleichungen der mathematischen Physik, Mathematische Annalen 100 (1) (1928) 32–74.
[2] R. Hartmann, F. Bassi, I. Bosnyakov, L. Botti, A. Colombo, A. Crivellini, M. Franciolini, T. Leicht, E. Martin, F. Massa, et al., Implicit methods, in: TILDA: Towards Industrial LES/DNS in Aeronautics, Springer, 2021, pp. 11–59.
[3] U. M. Ascher, S. Ruuth, B. Wetton, Implicit-Explicit methods for time-dependent partial differential equations, SIAM Journal on Numerical Analysis 32 (1995) 797–823.
[4] U. M. Ascher, S. Ruuth, R. Spiteri, Implicit-explicit Runge-Kutta methods for time-dependent partial differential equations, Applied Numerical Mathematics 25 (1997) 151–167.
[5] S. Boscarino, Error analysis of IMEX Runge-Kutta methods derived from differential-algebraic systems, SIAM Journal on Numerical Analysis 45 (2007) 1600–1621.
[6] S. Boscarino, G. Russo, On a class of uniformly accurate IMEX Runge-Kutta schemes and applications to hyperbolic systems with relaxation, SIAM Journal on Scientific Computing 31 (3) (2009) 1926–1945.
[7] L. Pareschi, G. Russo, Implicit-explicit Runge-Kutta schemes and applications to hyperbolic systems with relaxation, Journal of Scientific Computing 25 (1-2) (2005) 129–155.
[8] S. Boscarino, G. Russo, Asymptotic preserving methods for quasilinear hyperbolic systems with stiff relaxation: a review, SeMA Journal. Boletin de la Sociedad Española de Matemática Aplicada 81 (1) (2024) 3–49. doi:10.1007/s40324-024-00351-x.
URL https://doi.org/10.1007/s40324-024-00351-x
[9] S. Gottlieb, C.-W. Shu, E. Tadmor, Strong stability-preserving high-order time discretization methods, SIAM Review 43 (1) (2001) 89–112.
[10] R. Chan, A. Tsai, On explicit two-derivative Runge-Kutta methods, Numerical Algorithms 53 (2010) 171–194.
[11] E. Hairer, G. Wanner, Multistep-multistage-multiderivative methods for ordinary differential equations, Computing (Arch. Elektron. Rechnen) 11 (3) (1973) 287–303.

[12] D. Seal, Y. Güçlü, A. Christlieb, High-order multiderivative time integrators for hyperbolic conservation laws, Journal of Scientific Computing 60 (2014) 101–140.
[13] A. Moradi, A. Abdi, J. Farzi, Strong stability preserving second derivative general linear methods with Runge–Kutta stability, Journal of Scientific Computing 85 (1) (2020) 1.
[14] J. Chouchoulis, J. Schütz, J. Zeifang, Jacobian-free explicit multiderivative Runge–Kutta methods for hyperbolic conservation laws, Journal of Scientific Computing 90 (3) (2022) 96.
[15] J. Schütz, D. Seal, An asymptotic preserving semi-implicit multiderivative solver, Applied Numerical Mathematics 160 (2021) 84–101.
[16] S. Gottlieb, Z. J. Grant, J. Hu, R. Shu, High order strong stability preserving multiderivative implicit and IMEX Runge–Kutta methods with asymptotic preserving properties, SIAM Journal on Numerical Analysis 60 (1) (2022) 423–449.
[17] A. Moradi, A. Abdi, G. Hojjati, Strong stability preserving implicit and implicit–explicit second derivative general linear methods with RK stability, Computational and Applied Mathematics 41 (4) (2022) 135.
[18] J. Schütz, D. C. Seal, J. Zeifang, Parallel-in-time high-order multiderivative IMEX solvers, Journal of Scientific Computing 90 (54) (2022) 1–33.
[19] J. Zeifang, J. Schütz, D. Seal, Stability of implicit multiderivative deferred correction methods, BIT Numerical Mathematics (2022).
[20] A. Thenery Manikantan, J. Schütz, Multi-step Hermite-Birkhoff predictor-corrector schemes, Applied Numerical Mathematics 205 (2024) 281–295. doi:https://doi.org/10.1016/j.apnum.2024.07.011.
URL https://www.sciencedirect.com/science/article/pii/S0168927424001910
[21] J. Zeifang, A. Thenery Manikantan, J. Schütz, Time parallelism and Newton-adaptivity of the two-derivative deferred correction discontinuous Galerkin method, Applied Mathematics and Computation 457 (2023) 128198.
[22] D. A. Kopriva, Implementing spectral methods for partial differential equations: Algorithms for scientists and engineers, Springer Science & Business Media, 2009.
[23] S. Jin, Asymptotic preserving (AP) schemes for multiscale kinetic and hyperbolic equations: A review, Rivista di Matematica della Universita Parma 3 (2012) 177–216.
[24] F. Cordier, P. Degond, A. Kumbaro, An asymptotic-preserving all-speed scheme for the Euler and Navier-Stokes equations, Journal of Computational Physics 231 (2012) 5685–5704.
[25] S. Noelle, G. Bispen, K. Arun, M. Lukáčová-Medvid'ová, C.-D. Munz, A weakly asymptotic preserving low Mach number scheme for the Euler equations of gas dynamics, SIAM Journal on Scientific Computing 36 (2014) B989–B1024.
[26] G. Bispen, M. Lukáčová-Medvid'ová, L. Yelash, Asymptotic preserving IMEX finite volume schemes for low Mach number Euler equations with gravitation, Journal of Computational Physics 335 (2017) 222–248.
[27] E. Theodosiou, J. Schütz, D. Seal, An explicitness-preserving imex-split multiderivative method, Computers & Mathematics with Applications 158 (2024) 139–149. doi:https://doi.org/10.1016/j.camwa.2023.12.040.
URL https://www.sciencedirect.com/science/article/pii/S089812212400021X
[28] S. Klainerman, A. Majda, Singular limits of quasilinear hyperbolic systems with large parameters and the incompressible limit of compressible fluids, Communications on Pure and Applied Mathematics 34 (1981) 481–524.
[29] P. Degond, M. Tang, All speed scheme for the low Mach number limit of the isentropic Euler equation, Communications in Computational Physics 10 (2011) 1–31.
[30] J. Haack, S. Jin, J.-G. Liu, An all-speed asymptotic-preserving method for the isentropic Euler and Navier-Stokes equations, Communications in Computational Physics 12 (2012) 955–980.
[31] K. Kaiser, J. Schütz, R. Schöbel, S. Noelle, A new stable splitting for the isentropic Euler equations, Journal of Scientific Computing 70 (2017) 1390–1407.
[32] J. Schütz, D. Seal, A. Jaust, Implicit multiderivative collocation solvers for linear partial differential equations with discontinuous Galerkin spatial discretizations, Journal of Scientific Computing 73 (2017) 1145–1163.
[33] K. Kaiser, J. Schütz, Asymptotic error analysis of an IMEX Runge–Kutta method, Journal of Computational and Applied Mathematics 343 (2018) 139–154.
[34] J. Zeifang, J. Schütz, Implicit two-derivative deferred correction time discretization for the discontinuous Galerkin method, Journal of Computational Physics 464 (2022) 111353.
[35] M. Franciolini, A. Crivellini, A. Nigro, On the efficiency of a matrix-free linearly implicit time integration strategy for high-order discontinuous Galerkin solutions of incompressible turbulent flows, Computers & Fluids 159 (2017) 276–294.
[36] D. A. Knoll, D. E. Keyes, Jacobian-free Newton–Krylov methods: a survey of approaches and applications, Journal of Computational Physics 193 (2004) 357–397.
[37] N. Krais, A. Beck, T. Bolemann, H. Frank, D. Flad, G. Gassner, F. Hindenlang, M. Hoffmann, T. Kuhn, M. Sonntag, et al., FLEXI: A high order discontinuous Galerkin framework for hyperbolic–parabolic conservation laws, Computers & Mathematics with Applications 81 (2021) 186–219.
[38] G. Bispen, K. R. Arun, M. Lukáčová-Medvid'ová, S. Noelle, IMEX large time step finite volume methods for low Froude number shallow water flows, Communications in Computational Physics 16 (2014) 307–347.
[39] K. Kaiser, J. Schütz, A high-order method for weakly compressible flows, Communications in Computational Physics 22 (4) (2017) 1150–1174.
[40] J. Zeifang, K. Kaiser, A. Beck, J. Schütz, C.-D. Munz, Efficient high-order discontinuous Galerkin computations of low Mach number flows, Communications in Applied Mathematics and Computational Science 13 (2018) 243–270.
[41] William H. Press, S. A. Teukolsky, W. T. Vetterling, B. P. Flannery, Numerical recipes 3rd edition, 3rd Edition, Cambridge University Press, Cambridge, England, 2007.
[42] B. Cockburn, C. W. Shu, Runge-Kutta discontinuous Galerkin methods for convection-dominated problems, Journal of Scientific Computing 16 (2001) 173–261.